Clumped isotopes in globally distributed Holocene coccoliths reveal their habitat depth

Luz María Mejía[1,2*], Stefano M. Bernasconi[1], Hongrui Zhang[1], José Guitián[1,3], Alvaro Fernandez[1,4], Ivan Hernández-Almeida[1], Madalina Jaggi[1], Negar Haghipour[1], Heather Stoll[1]

[1] Geological Institute, ETH Zürich, Sonneggstrasse 5, ETH, 8092, Zürich, Switzerland.
[2] Now at MARUM, University of Bremen, 28359 Bremen, Germany
*corresponding author: lmejia@marum.de
[3] Now at Centro de Investigación Mariña, Universidade de Vigo, GEOMA, Vigo, 36310, Spain
[4] Now at Instituto Andaluz de Ciencias de la Tierra, Av. de las Palmeras, 4, 18100 Armilla, Granada, Spain

Clumped isotopes in globally distributed Holocene coccoliths reveal their habitat depth

Luz María Mejía[1,2], Stefano M. Bernasconi[1], Hongrui Zhang[1], José Guitián[1,3], Alvaro Fernandez[1,4], Ivan Hernández-Almeida[1], Madalina Jaggi[1], Negar Haghipour[1], Heather Stoll[1]

Reliable temperature reconstructions are necessary to improve climate reconstructions and comparisons with paleoclimate model simulations. Most existing paleotemperature proxies are based on organic and inorganic remains of marine organisms. Despite the evidence that the habitat depth of coccolithophores and other phytoplankton depend on their ability to balance light, nutrients, and grazing pressure, calibrations of proxies based on photosynthesizers often assume they live in the surface ocean. Here we present the first globally distributed dataset of core top multi-species coccolith clumped isotopes (Δ_{47}), which show a clear latitudinal thermal gradient and demonstrate coccolith Δ_{47} sensitivity to temperature. The application of the most recent Δ_{47}-temperature calibration for marine biogenic carbonates yield calcification temperatures implying deep habitats for tropical coccolithophores (from ~50 to up to ~150 m), which could photosynthesize with 1-10% of surface photosynthetic active radiation (PAR) levels. Given the low upper ocean temperature gradient of well-mixed high-latitude locations and the current uncertainties of Δ_{47} thermometry, coccolith Δ_{47} cannot be used to reliably constrain a specific habitat depth in these locations. Nevertheless, they are a good indicator of paleotemperatures of the mixed layer. We also use coccolith Δ_{47} to derive the first regression relating core top coccolith Δ_{47} and sea surface temperatures (SST). Although this formulation cannot be considered a proper coccolith-specific Δ_{47} calibration, since it ignores coccolithophore's potential for calcification at depth, it facilitates comparison

64 with temperature proxies like $U^{k\prime}_{37}$, which are regressed to SST, rather than production

65 temperature.

69 [1] Geological Institute, ETH Zürich, Sonneggstrasse 5, ETH, 8092, Zürich, Switzerland.
70 [2] Now at MARUM, University of Bremen, 28359 Bremen, Germany
71 [3] Now at Centro de Investigación Mariña, Universidade de Vigo, GEOMA, Vigo, 36310, Spain
72 [4] Now at Instituto Andaluz de Ciencias de la Tierra, Av. de las Palmeras, 4, 18100 Armilla, Granada,
73 Spain

76 **1. Introduction**

78   Estimates of past sea surface temperatures (SST) are an important paleoclimate proxy

79 goal. The most widely used geochemical SST proxies are either based on organic

80 biomarkers produced by coccolithophores (alkenone unsaturation index - $U^{k\prime}_{37}$) and

81 archaea (archaeal tetraether index -TEX_{86}-), or on biominerals produced by planktonic

82 foraminifera ($\delta^{18}O$, Mg/Ca and more recently, clumped isotopes -Δ_{47}-). Since alkenones

83 are produced by coccolithophores, which rely on light availability to photosynthesize and

84 lack any motile apparatus during their diploid phase, $U^{k\prime}_{37}$ is often assumed to be the most

85 reliable indicator of temperatures at the ocean's surface. Conversely, TEX_{86} may also

86 record subsurface ocean temperatures, as the archaea that produce these biomarkers can

87 live throughout the water column (Ho and Laepple, 2016; Rommerskirchen et al., 2011;

88 Schouten et al., 2013; Tierney et al., 2017), and even planktic foraminifera inferred to

89 dwell in the surface mixed layer may span depths from 15 to up to ~200 meters in different

90 oceanographic settings and seasons (Kretschmer et al., 2018; Rebotim et al., 2017).

91   Reconstructions of ocean temperatures from these proxies are used in climate models

92 to access their performance and to understand past climate evolution and Earth climate

93 sensitivity (e.g. Lunt et al., 2021; Zhu et al., 2019). However, if instead of SST, some of

94 these proxies were actually indicators of deeper water conditions, climate modelers

95   should consider depth differences in their calibration efforts. Plankton sampling shows

96   that placolith-bearing coccolithophores, including those of alkenone producers, are

97   present at depths ranging from the surface to 200-300 m in different ocean settings (Balch

98   et al., 2019; Beaufort et al., 2008; Liu et al., 2021; Poulton et al., 2017). While the

99   presence of cells at depth is not necessarily indicative of significant cell growth, the

100   shallowest layer is also not always favorable for growth because it can be nutrient-

101   depleted and high light intensities and UV radiation can damage photosystem II and

102   inhibit its repair cycle (Bouchard' et al., 2006; Guan and Gao, 2010). In addition to

103   alkenones, coccolithophores produce calcite platelets termed coccoliths, which are well

104   preserved in the geological record, and can be used to infer their habitat's conditions in

105   the past.

106   Clumped isotope (Δ_{47}) thermometry is a technique that estimates temperatures of

107   calcification by comparing the excess abundance of ^{13}C-^{18}O bonds in the carbonate with

108   that expected from a stochastic distribution (Eiler, 2011, 2007; Schauble et al., 2006). In

109   contrast to foraminiferal $\delta^{18}O$ and Mg/Ca, it is independent of seawater chemistry (Ghosh

110   et al., 2006), and Δ_{47} thermometry in planktic and benthic foraminifera is therefore

111   emerging as an important paleoceanographic proxy (e.g. Evans et al., 2018; Leutert et al.,

112   2020; Meckler et al., 2022; Meinicke et al., 2021, 2020; Peral et al., 2022, 2018; Piasecki

113   et al., 2019; Rodríguez-Sanz et al., 2017). Despite the abundance of coccoliths in

114   Cenozoic sediments and the constraint that they must be produced in the photic zone, the

115   potential of their Δ_{47} thermometry has not yet been rigorously evaluated in ocean sediment

116   samples. A culture study showed that coccolith Δ_{47} correlates closely with temperature

117   and found no significant differences in the relationship among different species (Katz et

118   al., 2017).

119   In order to verify the relationship between temperature and sedimentary coccolith

120   Δ_{47}, we measured Δ_{47} on globally distributed Holocene multispecies coccolith fractions,

121   which represent natural populations, and would be the most readily obtained fraction for

122   future paleoceanographic studies. We also use our coccolith Δ_{47} to evaluate

123   coccolithophores' habitat depth in different oceanographic settings. For this, we apply the

124   most recent biogenic Δ_{47} calibration (Meinicke et al., 2021) to derive coccolith

125   calcification temperatures. We then compare these temperatures with the vertical

126   distribution of ocean temperatures in the modern upper water column during the season

127   of production, and with alkenone $U_{37}^{k\prime}$-derived temperatures from the same samples

128   calculated using core top calibrations regressed to SSTs (Müller et al., 1998; Tierney and

129   Tingley, 2018). This assessment of likely calcification and habitat depth may improve

130   interpretation of temperatures attained from both alkenones and coccolith $\Delta_{47,}$ facilitating

131   more robust proxy intercomparison and more meaningful information for data-model

132   comparisons.

133

134   **2. Materials and Methods**
135

136   *2.1. Sediment samples*
137

138   We chose a set of 12 sites distributed around the world, including locations with

139   various oceanographic conditions (Fig. 1; Supplementary Table A). These comprised: a)

140   three tropical Equatorial Pacific sites influenced by upwelling (IODP U1337, IODP 1338,

141   and ODP 1226); b) two tropical oligotrophic sites, including one in the Caribbean

142   Colombian basin (ODP Site 999), and one in the southern South China Sea (ODP 1143);

143   c) three in the North Atlantic at mid-latitude (northeast of the Azores: IODP U1312) and

144   at high latitudes (Rockall Plateau: ODP 982, and Iceland Plateau: ODP 985); d) one in

the South Atlantic in the northwestern flank of the Walvis Ridge (ODP 1266); and e)

three in the Southern Ocean (western Pacific sector in the Subantarctic zone: ODP Site

1122, Atlantic sector in the Polar Frontal zone: ODP 1092, and Atlantic sector in the

Antarctic zone: ODP 1093). We targeted mid to late Holocene sediments with a modest

to high carbonate content so that microfiltration would yield sufficient coccolith fraction

for clumped isotope analyses. The age of each sample was determined by radiocarbon

analysis of mixed species of planktonic foraminifera (Supplemetary Table B) in the ETH

laboratory of Ion Beam Physics (LIP) following established methodologies (McIntyre et

al., 2017).
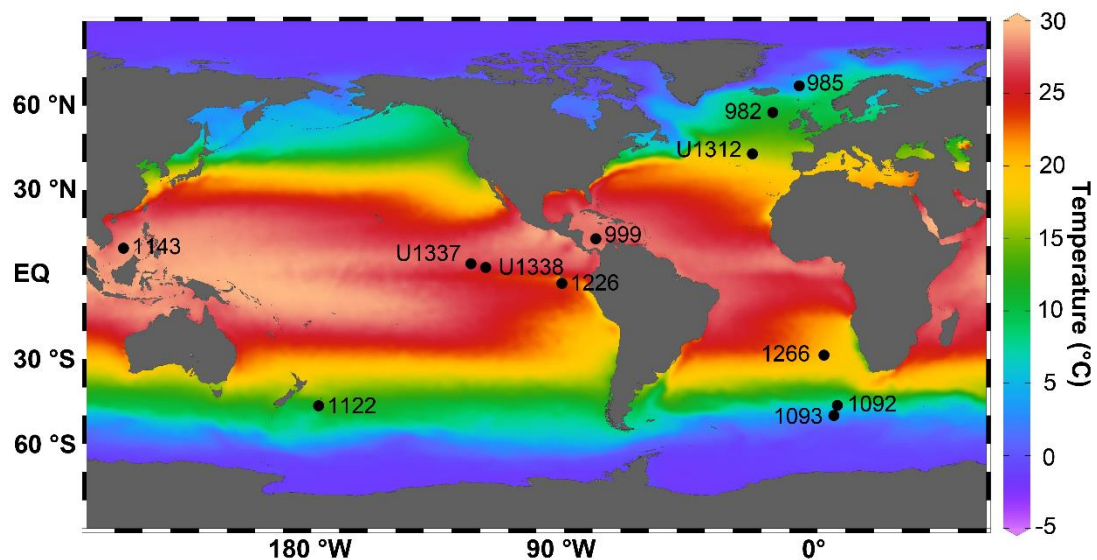
Fig. 1. Location of mid to late Holocene sediment Sites in this study on a global mean
surface temperature map (World Ocean Atlas -WOA, 2018) generated using ODV
(Schlitzer, 2021).

2.2. Alkenone thermometry

Freeze-dried bulk samples were extracted via accelerated solvent extraction, using a

5:1 mixture of dichloromethane (CH_2Cl_2) and methanol (MeOH) at 100°C in three 10-

minute static cycles, using a ThermoFisher 350 Accelerated Solvent Extractor (ASE). The

164 total lipid extract was separated into hydrocarbon, ketone and polar fractions using silica

165 gel column chromatography. The ketone fraction was analyzed following the methods

166 detailed in Guitián and Stoll (2021) using a Thermo Scientific Trace 1310 Gas

167 Chromatograph (GC) coupled to a flame ionization detector. The precision, estimated

168 from measurements of an in-house alkenone internal standard, was 0.012 $U_{37}^{k\prime}$ units

169 (0.36°C calculated with the calibration of Müller et al., 1998). Abundances of $C_{37:2}$ and

170 $C_{37:3}$ were used to calculate the alkenone unsaturation index ($U_{37}^{k\prime}$). We applied the most

171 widely used calibrations to estimate SSTs from $U_{37}^{k\prime}$, including the core top (Müller et al.,

172 1998), the Bayspline (Tierney and Tingley, 2018), and the 55a *Emiliania huxleyi* batch

173 culture (Prahl et al., 1988) calibrations. ODP Sites 999 and 1092 had insufficient

174 alkenones for temperature determination.

175

176 ***2.3. Coccolith clumped isotope thermometry***
177

178 *2.3.1. Organic matter removal*

179 The determination of clumped isotopic composition of carbonates by mass

180 spectrometry can be influenced by contaminants which produce isobaric interferences on

181 the m/z 47 ion beam. To eliminate potential contaminants, we used the bulk sediment

182 extracted for alkenone analysis, i.e. free of extractable lipids. From this material, we

183 obtained a coccolith-enriched <11 μm size fraction by microfiltration in an ammonia

184 solution (0.5%) pre-saturated with respect to carbonate. The remaining organic matter in

185 this fraction was oxidized for four hours using 500 mL of an ammonia-buffered (pH 8-9)

186 10% hydrogen peroxide (H_2O_2) solution. For organic carbon-rich samples (i.e. U1337

187 and U1338), a double oxidation step was necessary. To test if the extraction procedure

188 alters the isotopic composition of the samples, we applied the ASE extraction to the

189　international standard ETH 3 because it is a chalk mainly composed of coccoliths, and is

190　very similar to our samples (Bernasconi et al., 2021). The H_2O_2 oxidation was tested in a

191　randomly-chosen sample from which we had abundant material (ODP Site 1266). No

192　effect was observed on measured $\delta^{18}O$, $\delta^{13}C$ and Δ_{47} after solvent extraction nor H_2O_2

193　oxidation (Supplementary Table C).

194

195　*2.3.2. Coccolith size fraction separation*

196　　Since all samples were younger than 8700 years (Supplementary Table B), we expect

197　negligible input of authigenic carbonate in the small fraction (<2 µm). Therefore, for most

198　samples we did not eliminate the <2 µm fraction. Rather, we aimed to limit the

199　contribution from large fragments of non-coccolith carbonate, such as foraminifera. We

200　used light microscopy to determine the largest coccolith size, which would exclude

201　foraminifera fragments. When necessary, the <11 µm fraction was filtered again at 8 or

202　10 µm. The filtered samples were then washed three times in Milli-Q water to eliminate

203　the ammonia, dried at 50° C, and homogenized prior to Δ_{47} analysis.

204　　We attempted to eliminate the <3 µm size fraction in the two tropical oligotrophic

205　samples (ODP Site 999 and 1143), as light microscopy showed they were enriched in the

206　deep photic species *Florisphaera profunda*. We used a mix of centrifugation (seven

207　repetitions at 2800 RPM for 2 minutes, to eliminate fragments <2 µm) (Zhang et al., 2021)

208　followed by microfiltration at 3 µm. Due to the small sample size, we could not obtain

209　enough purified 3-8 µm coccoliths for ODP Site 999, and therefore we report the Δ_{47}

210　results of the <11 µm fraction.

211　　The presence of non-coccolith carbonate, like foraminifera fragments, could bias Δ_{47}-

212　temperature estimations, since they may not share the same habitat temperature. We used

213　scanning electron microscopy (SEM) and trace element analysis (Sr/Ca, Mg/Ca, Al/Ca

214 and Mg/Al) to determine if non-identifyable fragments, mostly of sizes <2 µm, were

215 originated from broken coccolithophores or foraminifera. Results are shown in

216 Supplementary Note A, Table D, and Fig. A. For this, we dissolved 300-380 µg of final

217 coccolith separations using 2% HNO_3 for ∼15 min, and determined element ratios using

218 an Agilent 8800 Triple Quadrupole ICP-MS, using intensity ratio calibration as described

219 in Mejía et al. (2014).

220

221 *2.3.3. Clumped isotope measurements*

222   Clumped isotopes, $\delta^{18}O$ and $\delta^{13}C$ from coccolith separations were measured using a

223 Kiel IV-Thermo Fisher Scientific MAT 253 system with the LIDI protocol (Müller et al.,

224 2019). The Kiel IV device includes a custom built PoraPakQ trap held a –40 °C to

225 eliminate potential organic contaminants. Prior to each sample run, the pressure-

226 dependent backgrounds are determined on all beams to correct for non-linearity effects

227 in the mass spectrometer. During each run of 46 positions, 3 replicates of 8 different

228 samples, 5 replicates of the carbonate standards ETH-1 and ETH-2, and 10 replicates of

229 ETH-3, are analyzed for data normalization. Two replicates of the international standard,

230 IAEA C2, are analyzed with each run to monitor the long-term reproducibility of the

231 method. For each sample of this study 11-21 replicate measurements (average of 15) were

232 conducted, with sample amounts adjusted to yield 90-110 µg of $CaCO_3$ per replicate.

233 Samples were measured over 19 months and the data were processed with the software

234 Easotope (John and Bowen, 2016). Replicates with 49-parameter values (John and

235 Bowen, 2016) >2 or Δ_{48} offset > 2 ‰ were discarded due to potential sample

236 contamination.

237   We report Δ_{47} in the I-CDES scale which is defined with the three carbonate standards

238 ETH-1 (Δ_{47}=0.2052‰), ETH-2 (Δ_{47}=0.2085‰), and ETH-3 (Δ_{47}=0.6132‰) (Bernasconi

239   et al., 2021). Long-term external standard deviation of the international standard IAEA

240   C2 was: $\delta^{13}C$=0.03 ‰, $\delta^{18}O$=0.04‰, Δ_{47}=0.024 ‰; n = 322. Analytical errors of Δ_{47}

241   estimates are reported at the 95% confidence interval (CI) (Fernandez et al., 2017).

242

243   *2.3.4. Estimation of coccolith calcification temperatures from Δ_{47}*

244   The most reliable estimates of coccolith calcification temperatures would be achieved

245   by applying a statistically well-constrained Δ_{47}-calibration based on coccolithophores

246   grown at known temperatures, and normalized to the I-CDES using carbonate

247   standardization. Unfortunately, the only published coccolith-specific calibration (Katz et

248   al., 2017) was carried out before the introduction of the I-CDES standardization. Thus,

249   calcification temperatures estimated with this calibration have a poorly constrained

250   source of uncertainty (Bernasconi et al., 2021). In addition, it only includes a small

251   number of samples (n=11) with limited replication and a limited range of growth

252   temperatures, which increases the uncertainty of the slope and of the confidence interval.

253   Therefore, we estimated coccolith calcification temperatures using this calibration, but

254   due to the uncertainties, we discuss them only in the Supplementary Information.

255   The latest published abiogenic carbonate Δ_{47} calibration (Anderson et al., 2021) has

256   the advantage of using the same carbonate standardization (ETH-1, 2 and 3) and

257   processing techniques as those used in this study. To reduce a possible bias induced by

258   the few high temperature datapoints (1-2 °C) we recalculated the published equation using

259   the regression of York et al. (2004) applied to the subset of 23 laboratory-grown and

260   natural samples, which included only temperatures relevant for coccolithophore

261   environments (0.5-36.1 °C). The larger number of datapoints of this calibration translates

262   into smaller uncertainties in temperature estimates. Moreover, temperatures used for this

263   calibration are experimentally determined or directly measured. The main disadvantage

264 is that this calibration is only based on abiogenic calcite, and biomineralization is a

265 process which could deviate from the expected equilibrium Δ_{47}-temperature relationships

266 (e.g. some corals; Fiebig et al., 2021; Spooner et al., 2016).

267 The latest foraminiferal core-top based clumped isotope calibration (Meinicke et al.,

268 2021) includes globally distributed planktonic and benthonic species (Meinicke et al.,

269 2020; Peral et al., 2018; Piasecki et al., 2019) , and is directly comparable to our data, as

270 standardization, correction and processing followed the same methodology. Although not

271 derived from coccolithophore calcite, this calibration does consider potential effects of

272 biomineralization. The main uncertainty of this calibration is that the used temperature is

273 not experimentally-derived or directly measured, but rather calculated from foraminifera

274 oxygen isotope composition. However, it includes by far the largest sample set (n=78)

275 and replicate numbers, rendering the calibration the most statistically robust.

276 Furthermore, it has been applied to extinct biomineralizers or other organisms which are

277 not part of the calibration set, under the assumption that the regression is relevant broadly

278 for marine biomineralization (Agterhuis et al., 2022; Caldarescu et al., 2021; Leutert et

279 al., 2021; Meckler et al., 2022). Based on the above considerations, we will focus on

280 calcification temperatures estimated using the Meinicke et al. (2021) calibration, which,

281 until a coccolith-specific calibration is available, can be considered the most reliable (see

282 also Meckler et al., 2022).

283

284 *2.4. Reconstruction of coccolithophores' habitat depth*
285

286 Possible coccolith calcification temperatures for each location are defined by the

287 temperature range in the euphotic zone during the season of maximum production.

288 Therefore, assuming no significant vital effects on coccolith Δ_{47}, as suggested by all

289   previous studies (Drury and John, 2016; Katz et al., 2017; Tagliavento et al., 2019; Tripati

290   et al., 2010), we use the calcification temperatures determined with the Meinicke et al.

291   (2021) calibration to estimate the average habitat depth of coccolithophores at each

292   location. This is done by comparing the Δ_{47}-calcification temperature with the vertical

293   temperature distribution in the water column during the season of main coccolithophore

294   production for each Site, which is taken from the World Ocean Atlas -WOA- (2018). The

295   shallowest and deepest limits are determined from the warmest and coldest Δ_{47}-

296   temperatures determined from the temperature uncertainty at the 95% CI.

297   Previous studies of Δ_{47} in monospecific planktic foraminifera have relied on $\delta^{18}O$

298   measurements and used species-specific $\delta^{18}O$ paleotemperature equations to estimate

299   their calcification depth (Meinicke et al., 2020). However, this approach cannot be

300   applied to our polyspecific coccolith samples, because, as for planktic foraminifera

301   (Spero et al., 2003), different species of coccolithophores feature significantly different

302   $\delta^{18}O$ paleotemperature equations (Hermoso et al., 2015, 2014).

303

304   *2.4.1. Selection of coccolithophores' main season of production*

305   The production temperature of coccoliths at a given location is not precisely known

306   because coccolithophores may calcify at a range of depths in the euphotic zone, and

307   production may be concentrated in a particular season. Where limited by nutrients, for

308   instance in areas of the subtropical and tropical oceans, productivity may be strongest

309   during periods of de-stratification, a process which supplies nutrients and leads to cooler

310   temperatures. On the other hand, where light is limiting, like at very high latitudes,

311   primary producers generally show their highest biomass during warmest periods

312   (Dandonneau et al., 2004).

313   We estimated the main season of production for each location from a variety of

314   approaches. Where available, we relied on direct production estimates such as satellite-

315   based chlorophyll *a* concentration and sediment trap coccolithophore fluxes.

316   Additionally, we used oceanographic data obtained during cruises (e.g. using CTD

317   stations) and floats, which elucidate the nutrient and physical controls on production, as

318   well as models of production. The detailed information is provided in the Supplementary

319   Note B and Supplementary Figs. B-E.

320

321   *2.5. Construction of core top coccolith Δ$_{47}$-SST regression*
322

323   We derive a core top coccolith Δ$_{47}$-SST regression with a similar approach as that used

324   to establish the empirical calibration of the $U^{k'}_{37}$ thermometer, using SSTs (±1SE) of the

325   season of production for each site (WOA, 2018), and our coccolith Δ$_{47}$ measurements,

326   and by applying the regression method of York et al. (2004).Click or tap here to enter

327   text.Since this formulation does not consider the potential for coccolith calcification at

328   depth, which could be significantly colder than at surface at some locations, this core top

329   coccolith Δ$_{47}$-SST equation is not analogous to the Δ$_{47}$ calibrations mentioned above

330   (Anderson et al., 2021; Katz et al., 2017; Meinicke et al., 2021), and should therefore not

331   be considered as a coccolith-specific calibration. However, we explore this approach for

332   comparison to temperatures derived from core top $U^{k'}_{37}$-SST calibrations.

333

334   **3. Results**
335

336   *3.1. Coccolith clumped and stable oxygen and carbon isotopes*
337

338   Coccolith Δ_{47} decreases with increasing temperatures and ranges between 0.606 and

339   0.662 ‰ (I-CDES) (Table 1a, Fig. 2). These values are lower (warmer) and less variable

340   than Δ_{47} values of globally-distributed core top foraminifera species, which vary between

341   0.653 and 0.756 ‰ (Meinicke et al., 2020) . Despite the inherent difficulties of comparing

342   datasets generated using different standards, Δ_{47} and $\delta^{18}O$ values of the coccolithophore

343   culture work of Katz et al. (2017), in which growth temperatures are similar to those we

344   expect for our samples (7 to 25 °C), are similar in both magnitude and range of variation

345   to our core top coccolith Δ_{47} and $\delta^{18}O$ values. Coccolith $\delta^{18}O$ varied by 5.5‰ (between -

346   1.97 and 3.48 ‰, Table 1a, Fig. 2a).

347   Compared to $\delta^{18}O$, the range of variation of our coccolith $\delta^{13}C$ was smaller (from -

348   0.01 to 1.36 ‰, Table 1a, Fig. 2b), except for one sample in the South Atlantic (3.03 ‰).

349   Preindustrial $\delta^{13}C$ of dissolved inorganic carbon (DIC) in the surface ocean in regions

350   represented by our core tops is simulated to vary spatially by less than 1.6‰ (Eide et al.,

351   2017). Our core top samples therefore appear to manifest a smaller range of $\delta^{13}C$ vital

352   effects (coccolith $\delta^{13}C$- $\delta^{13}C_{DIC}$) than observed among different species (5.7 ‰) in the

353   culture study of Katz et al. (2017). Coccolith Δ_{47} and coccolith $\delta^{18}O$-$\delta^{18}O_{sw}$ show a

354   significant positive correlation (r = 0.84, p = 0.0007; Fig. 2a). Since vital effects in

355   coccolith $\delta^{13}C$ and $\delta^{18}O$ of a given species in cultures often correlate positively (e.g.

356   Ziveri et al., 2003), as is the case for the cultures of Katz et al. (2017), a small vital effect

357   in our coccolith $\delta^{13}C$ suggests likewise a small vital effect on $\delta^{18}O$.

358   Despite the relatively small inferred $\delta^{18}O$ vital effects in our dataset, calculating

359   growth temperature and water depth habitats from coccolith $\delta^{18}O$ would not lead to more

360   precise estimates. The variable oxygen isotope fractionations of different species and

361   potential presence of environmental-driven variation in vital effects of a given species

362 (Hermoso et al., 2015, 2014) does not allow isolating temperature from vital effect

363 influences in coccolith $\delta^{18}O$.

364

365

366

367

368

369

370

371

372

373

374

375
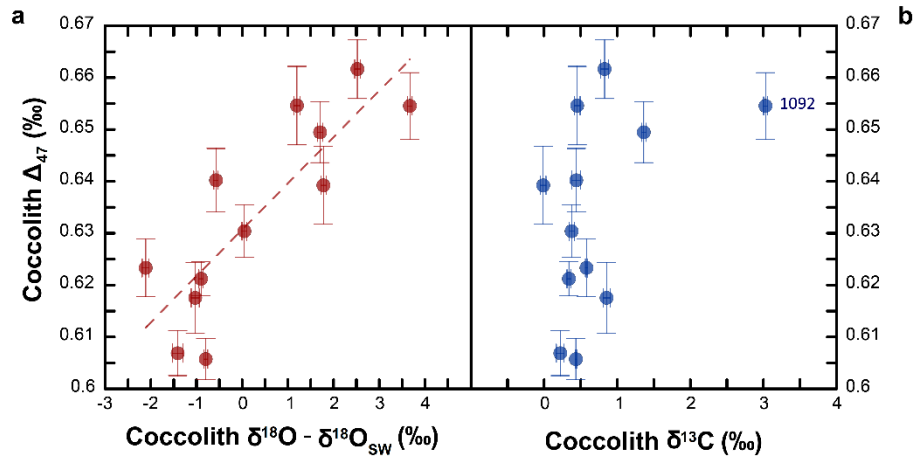
376 **Fig. 2.** Clumped isotopes (Δ_{47}, ‰) of coccolith separations as a function of **a)** coccolith

377 $\delta^{18}O$ minus $\delta^{18}O$ of seawater ($\delta^{18}O$-$\delta^{18}O_{SW}$); where $\delta^{18}O$ of coccoliths is with respect to

378 V-PDB and $\delta^{18}O_{SW}$ is with respect to V-SMOW, and **b)** coccolith $\delta^{13}C$. Seawater $\delta^{18}O$

379 used to calculate $\delta^{18}O$-$\delta^{18}O_{SW}$ are surface values from LeGrande and Schmidt (2006), and

380 are similar to values to up to 50-100 m depth, depending on the Site. The positive

381 correlation between coccolith Δ_{47} and $\delta^{18}O$ is statistically significant (r = 0.84, p =

382 0.0007). Error bars define one standard error of the Δ_{47} and one standard deviation of the

383 $\delta^{18}O$ and $\delta^{13}C$.

384

385 *3.2. SST during main season of production vs. $U_{37}^{k'}$ SST temperatures*

386

387   Sea surface temperatures (0 m) WOA (2018) during the determined main season of

388 peak production are reported in Table 1. For the tropical Equatorial Pacific locations,

389 SSTs ranged from 20.9 to 25.8 °C, while those of the tropical oligotrophic sites were

390 higher (26.6-27.5 °C). For the North Atlantic, peak production SSTs ranged from 14.5 °C

391 at the mid-latitude IODP Site 1312 to 6.9 °C at our northernmost ODP Site 985. SSTs at

392   the South Atlantic and Southern Ocean locations varied from 17.5 °C (ODP Site 1266) to

393   4.1 °C (ODP Site 1093). $U_{37}^{k\prime}$ ratios varied between 0.330 and 0.965 (Table 1a), showing

394   a clear latitudinal gradient. Although the calculated $U_{37}^{k\prime}$ temperature correlates with

395   SSTs, regardless of the calibration used, $U_{37}^{k\prime}$ -derived temperatures (Table 1b)

396   overestimate modern ocean SSTs of coccolithophore production season for most sites

397   analyzed, with the largest differences generally observed at the highest latitudes and areas

398   influenced by strong upwelling (Fig. 3, Supplementary Fig. F).

399

400   **Table 1. a)** Site, size fraction, ocean region, average and variation of the base of the mixed

401   layer (MLD; m), and average SST (0 m, °C) during the season of production (Seas. Prod.),

402   Δ_{47} value with standard error (‰) and number of replicates (n), alkenone unsaturation

403   index ($U_{37}^{k\prime}$), and oxygen ($\delta^{18}O$) and carbon ($\delta^{13}C$) isotopic composition with standard

404   deviation (‰, VPDB). SSTs and their respective standard deviations (SD) were obtained

405   from WOA (2018). **b)** SST (°C) obtained using the core top[1] (Müller et al., 1998),

406   bayspline[2] (Tierney and Tingley, 2018), and strain 55a *Emiliania huxleyi* batch culture[3]

407   (Prahl et al., 1988) alkenone calibrations, calcification temperatures (CT; °C) obtained

408   using the planktonic foraminifera[1] (Meinicke et al., 2021), the abiogenic[2] (Anderson et

409   al., 2021), and the coccolithophore culture[3] (Katz et al., 2017) Δ_{47} calibrations, including

410   uncertainties at the 95% CI, and average inferred habitat depth of coccolithophores (m)

411   using the foraminifera Δ_{47} calibration to derive CT. * indicate Sites where including the

412   95% CI of estimated calcification temperatures, these are colder or warmer than SSTs

413   during the season of production.

a

Site	Size fraction	Location	Seas. Prod.	MLD (m)	SST ± SD (°C)	Δ_{47} ± SE (‰)	n	$U^{k'}_{37}$	$\delta^{18}O$ ± SD (‰)	$\delta^{13}C$ ± SD (‰)
1093	<8	SO (Atl.)	Dec-Mar	69 (61-81)	4.12 ± 0.1	0.662 ± 0.006	12	0.330	2.27 ± 0.06	0.83 ± 0.06
1092	<8	SO (Atl.)	Nov-Feb	55 (49-65)	6.34 ± 0.1	0.655 ± 0.006	18		3.48 ± 0.05	3.03 ± 0.03
1122	<8	SO (West. Pac)	Dec-Jan	34 (32-36)	13.88 ± 0.1	0.655 ± 0.008	13	0.494	1.35 ± 0.06	0.45 ± 0.04
1266	<8	South Atlantic	Aug-Sep	78 (69-87)	17.46 ± 0.0	0.640 ± 0.006	17	0.691	0.10 ± 0.05	0.44 ± 0.06
1226	<8	Eq. Pacific	Aug-Sep	30 (28-31)	20.92 ± 0.2	0.621 ± 0.003	12	0.872	-0.61 ± 0.05	0.34 ± 0.03
U1338	<11	Eq. Pacific	Aug	29	24.67 ± 0.3	0.607 ± 0.004	11	0.965	-1.16 ± 0.11	0.22 ± 0.05
U1337	<11	Eq. Pacific	Aug	37	25.82 ± 0.0	0.606 ± 0.004	17	0.963	-0.54 ± 0.04	0.43 ± 0.01
1143	3-8	South China Sea	Dec-Mar	27 (25-31)	27.48 ± 0.2	0.623 ± 0.006	17	0.961	-1.97 ± 0.07	0.58 ± 0.01
999	<11	Colombian Car.	Jan-Mar	41 (40-42)	26.61 ± 0.1	0.618 ± 0.007	12		-0.25 ± 0.09	0.85 ± 0.05
U1312	<10	N. Atl. (Azores)	Apr-May	52 (36-69)	14.51 ± 0.3	0.630 ± 0.005	19	0.580	0.78 ± 0.05	0.38 ± 0.04
982	<10	N. Atl.	Dec-Jun	163 (29-261)	9.56 ± 0.3	0.649 ± 0.006	21	0.555	2.15 ± 0.06	1.36 ± 0.03
985	<10	N. Atl.	Jul	20	6.93 ± 0.6	0.639 ± 0.008	12	0.402	1.95 ± 0.06	-0.01 ± 0.04

b

Site	Location	SST ± SD (°C)	$U^{k'}_{37}$ SST¹ (°C)	$U^{k'}_{37}$ SST² (°C)	$U^{k'}_{37}$ SST³ (°C)	Δ47 CT¹ ± CI (95%) (°C)	Δ47 CT² ± CI (95%) (°C)	Δ47 CT³ ± CI (95%) (°C)	Inferred depth (m)
1093	SO (Atl.)	4.12 ± 0.1	8.7	8.1	8.6	6.0 ± 3.4	1.8 ± 4.2	6.3 ± 4.3	0
1092	SO (Atl.)	6.34 ± 0.1				8.2 ± 3.8	4.5 ± 4.7	9.1 ± 4.9	0
1122	SO (West. Pac)	13.88 ± 0.1	13.6	12.9	13.4	8.1 ± 4.6	4.5 ± 5.7	9.1 ± 5.9	284*
1266	South Atlantic	17.46 ± 0.0	19.6	18.8	19.2	12.2 ± 3.9	9.6 ± 5.0	14.3 ± 5.2	292*
1226	Eq. Pacific	20.92 ± 0.2	25.1	24.6	24.5	17.7 ± 2.3	16.4 ± 2.9	21.4 ± 3.0	50
U1338	Eq. Pacific	24.67 ± 0.3	27.9	29.7	27.2	22.3 ± 3.0	22.3 ± 3.9	27.5 ± 4.0	61
U1337	Eq. Pacific	25.82 ± 0.0	27.8	29.2	27.2	22.7 ± 2.7	22.9 ± 3.6	28.1 ± 3.7	95
1143	South China Sea	27.48 ± 0.2	27.8	29.2	27.1	17.3 ± 3.6	15.9 ± 4.7	20.9 ± 4.8	152
999	Colombian Car.	26.61 ± 0.1				19.1 ± 4.7	18.3 ± 6.1	23.3 ± 6.3	179
U1312	N. Atl. (Azores)	14.51 ± 0.3	16.2	15.5	15.9	15.1 ± 3.2	13.1 ± 4.1	18.0 ± 4.2	0
982	N. Atl.	9.56 ± 0.3	15.5	15.0	15.2	9.6 ± 3.5	6.3 ± 4.3	10.9 ± 4.4	0
985	N. Atl.	6.93 ± 0.6	10.9	10.2	10.7	12.5 ± 4.8	9.9 ± 6.0	14.7 ± 6.2	0*

4. Discussion

As photosynthetic organisms, coccolithophores need to balance their supply of nutrients and light, and grazing pressure to grow (Arteaga et al., 2020; Behrenfeld et al., 2013; Mignot et al., 2018). Therefore, their preferred habitat depth depends on the ability of each species to achieve such a balance. Peak coccolithophore cell abundance is typically located right above the deep chlorophyll maximum (DCM), which coincides with the lower limit of the euphotic zone along a meridional transect in the Atlantic Ocean across temperate, subtropical gyres and equatorial regions (Balch et al., 2019; Poulton et al., 2017). Deeper than surface production also agrees with maximum coccolithophore concentrations at the South Pacific Gyre between 200-300 m (Beaufort et al., 2008) and in the tropical Indian Ocean (Liu et al., 2021). It remains to be solved whether these cells can grow with 10-1% of surface photosynthetic active radiation (PAR), or if they are senescent from surficial blooms. Our Δ_{47}-derived calcification temperatures provide new insights on this question because they give an indication of potential habitat depths in different oceanic settings.

4.1. Δ_{47} calibration used for estimating calcification temperatures

While considering the uncertainties of comparing temperature estimates derived from carbonate (Anderson et al., 2021; Meinicke et al., 2021) vs. gas (Katz et al., 2017) standardized Δ_{47} calibrations, the application of these calibrations to our coccolith Δ_{47} dataset does lead to up to 5.3 °C differences in calculated calcification temperatures (Table 1b). In general, the warmest temperatures are obtained with the calibration of Katz et al. (2017), while temperatures using the calibration of Anderson et al. (2021) are the

454   coldest (Table 1b). The mixed foraminifera calibration (Meinicke et al., 2021) overall

455   leads to less extreme temperatures.

456   Continued improvements in analytical precision and interlaboratory comparability

457   may evaluate if there are small, not yet detectable, vital effects in coccolith Δ_{47}. A more

458   statistically robust coccolith-specific calibration could help to reduce uncertainties in the

459   calculated temperatures from coccolith Δ_{47}. Given the current state of knowledge and

460   absence of detected vital effects specific to coccolith biomineralization, we apply the

461   recent foraminifera calibration of Meinicke et al. (2021) to our coccolith Δ_{47} for reasons

462   detailed in section 2.3.4. In the following sections we discuss only temperatures derived

463   from this calibration, while results derived from Anderson et al. (2021) and Katz et al.

464   (2017) can be found in Table 1 and Supplementary Note C, Fig. G and H.

465

466   ***4.2. Coccolith Δ_{47}-derived calcification temperatures and coccolithophore's habitat depth***
467

468   Coccolith Δ_{47} calcification temperatures show a clear latitudinal gradient (Fig. 3a).

469   Except for ODP Site 985, Δ_{47}-derived temperatures are colder than temperatures obtained

470   using $U^{k\prime}_{37}$ (Fig. 3c). Δ_{47} temperatures are either colder (low latitudes) or fall close to SSTs

471   (mid-high latitudes). If the application of the foraminifera calibration (Meinicke et al.,

472   2021) to our data is correct, and there is no significant additional vital effect in coccolith

473   Δ_{47}, the calculated calcification temperatures indicate that coccolith calcification may

474   take place within the euphotic zone but at a significant depth in some regions of the

475   modern/Holocene ocean (Fig. 3b).

476   SEM observations do not show evidence of abiogenic carbonate overgrowth on

477   coccoliths (Supplementary Note A, Fig. A). Moreover, Sr/Ca ratios of the analyzed

478   fractions are consistent with those of coccolith calcite (e.g. Mejía et al., 2014, and refs.

479   therein), and exclude the presence of significant amounts of calcite precipitated from

480   seawater or pore fluids (Richter and Liang, 1993) in our samples (Supplementary Table

481   D). This suggests that fragments of unidentifiable origin are likely fragments from

482   coccoliths rather than authigenic carbonate. Therefore, the colder calcification

483   temperatures compared to SSTs of all our tropical Sites, and of ODP Sites 1122 and 1266,

484   are likely not a consequence of diagenetic alteration. Although some tropical samples

485   included subeuphotic zone coccolith species like *F. profunda* and *Ceratholitus cristatus,*

486   the contribution of subeuphotic carbonate is less than 17% (Supplementary Figure I).

487   Therefore, the potential cold signal introduced by their presence cannot explain by itself

488   the large magnitude of difference between SSTs and coccolith Δ_{47}-derived temperatures

489   (e.g. 7.5 °C for Site 999) (Supplementary Note D).
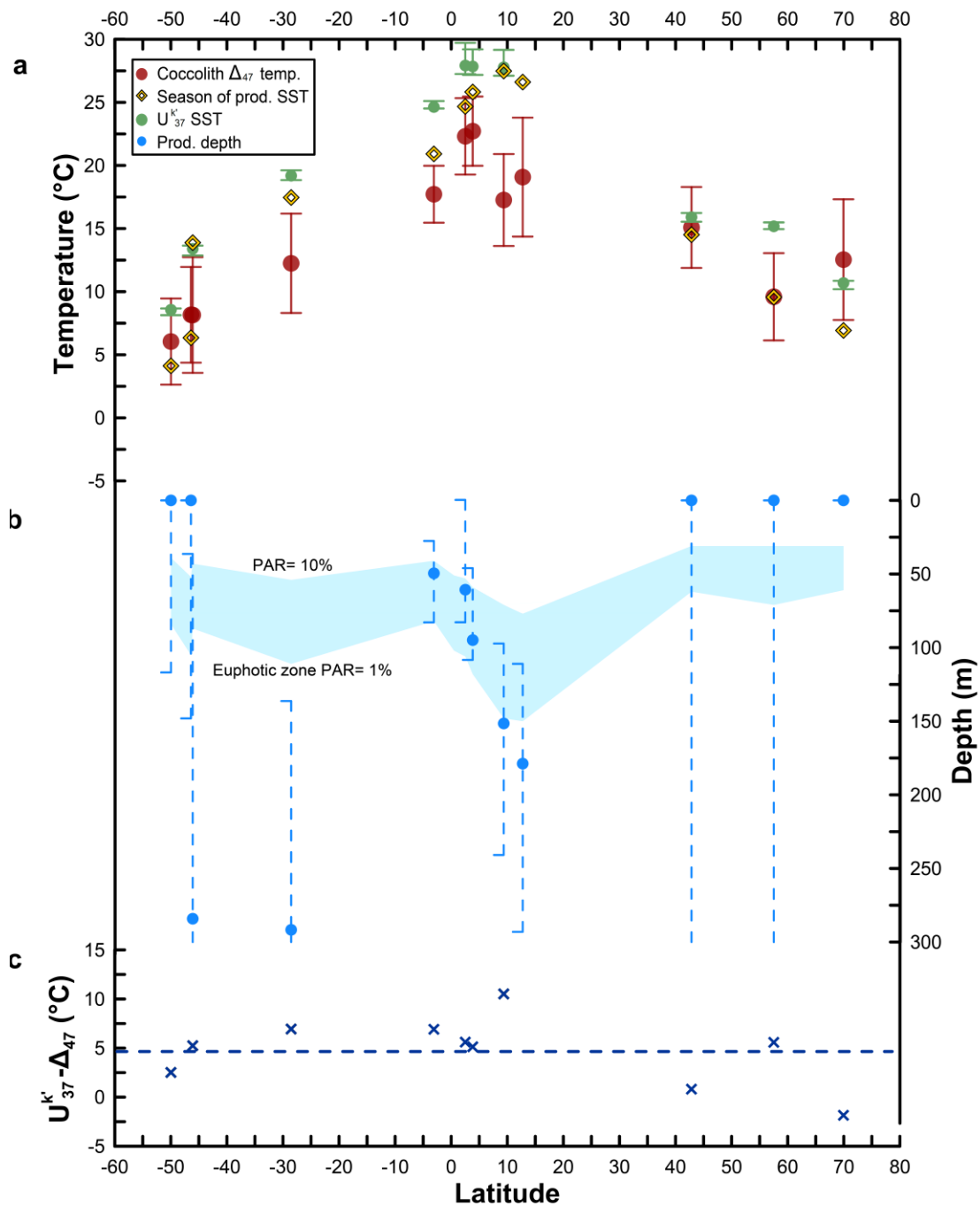
Fig. 3. a) Calcification temperatures (±95% CI) from coccolith Δ_{47} calculated with the foraminifera calibration (Meinicke et al., 2021) (red circles), SSTs from $U^{k'}_{37}$ (green circles), and average WOA SSTs during peak production months (yellow diamonds). $U^{k'}_{37}$ SSTs were estimated using the core top (Müller et al., 1998), bayspline (Tierney and Tingley, 2018), and the 55a *Emiliania huxleyi* batch culture (Prahl et al., 1988) calibrations, and error bars denote the maximum and minimum SST values. **b)** Coccolithophore habitat depths inferred from coccolith Δ_{47} calcification temperatures. Error bars indicating the potential shallowest and deepest habitat depths are calculated

499   using the warmest and coldest Δ_{47}-temperatures from the 95% CI extremes. Open error

500   bars denote a > 300 m depth limit. Depths below the euphotic zone are unrealistic. The

501   blue shaded area denotes depths where PAR ranges between 10-1%. **c)** Difference

502   between $U_{37}^{k\prime}$-annual SSTs and coccolith Δ_{47}-temperatures (blue cross). This calculation

503   considers $U_{37}^{k\prime}$-SSTs estimated using the calibration that leads to medium values

504   compared to the other two calibrations. Blue dashed line shows that on average $U_{37}^{k\prime}$-

505   annual SSTs are 4.7 °C warmer than coccolith Δ_{47}-temperatures.

506

507   *4.2.1. Tropical Pacific upwelling and tropical oligotrophic ocean regions*

508   Phytoplankton is recognized to grow throughout the euphotic zone (Behrenfeld et al.,

509   2013). The 2.4-3.2 °C and the 7.5-10.2 °C colder coccolith Δ_{47} calcification temperatures

510   compared to SSTs during the season of production at tropical upwelling and tropical

511   oligotrophic sites (Fig. 3a), respectively, are consistent with a deeper than surface habitat

512   in these regions (Fig. 3b; Table 1). In tropical regions with a strong thermocline and a

513   shallow mixed layer, the abundance of placolith-bearing coccolithophores, including

514   alkenone producers, has been shown to peak well below the surface. In the South Pacific

515   gyre, highest cell abundances are found at 200 m depth (Beaufort et al., 2008), while in

516   northern and southern oligotrophic regions of the Atlantic and in the Equatorial Atlantic,

517   peaks in coccosphere abundance follow a ~45 m thick layer just above the DCM (1%

518   PAR; lower limit of euphotic zone) (Poulton et al., 2017). This habitat distribution is

519   likely a consequence of nutrient depletion in the surface layers, combined with the ability

520   of most coccolithophores to obtain enough light at depths just above the lower limit of

521   the euphotic zone. Our coccolith Δ_{47}-calcification temperatures from all tropical sites are

522   consistent with the hypothesis that coccospheres and coccoliths retrieved at depth (e.g.

523   Beaufort et al., 2008; Cortés et al., 2001; Poulton et al., 2017) are not senescent cells, but

524   are rather actively growing and calcifying cells adapted to low light conditions.

525   Coccolith Δ_{47}-calcification temperatures in all Equatorial Pacific Sites (IODP U1337,

526   U1338 and ODP 1226) suggest that coccolithophore habitats are located above the lower

527   limit of the euphotic zone, but well below the surface, at depths between 50-95 m (Table

528   1b). Inferred habitat depths from Equatorial Pacific coccolith Δ_{47} temperatures agree

529   within error with depths where light levels fall between 10 and 1% PAR (average values

530   ranging from 14 to 41 $\mu E\ m^{-2}\ s^{-1}$) (Fig. 3b, Fig. 4a, b, c), which is consistent with highest

531   coccosphere abundance and diversity of low euphotic zone species in Equatorial regions

532   (Poulton et al., 2017).

533   Considering the relatively large uncertainties in coccolith Δ_{47}-temperatures of both

534   oligotrophic tropical sites (ODP 999: $\pm$ 4.7°C and 1143: $\pm$ 3.6 °C), and that especially for

535   Site 999, the $CaCO_3$ contribution of the subeuphotic species *F. profunda* (~17%) is

536   expected to have introduced a cold bias in calcification temperatures (Supplementary

537   Note D, Supplementary Fig. I)*,* coccolith Δ_{47}-inferred habitat depths also agree within

538   error with depths where light levels vary between 10% and 1% (Fig. 3b, Fig. 4d, e). Δ_{47}-

539   calcification temperatures at Sites 999 and 1143 would be expected to suggest deeper

540   habitats, closer to the lower limit of the euphotic zone at ~150 m, compared to the more

541   productive Equatorial Pacific regions (from 50-95 m). These observations are consistent

542   with deeper coccosphere abundance peaks in oligotrophic regions (~140 m) vs.

543   Equatorial areas (~70 m) of the Atlantic (Poulton et al., 2017).
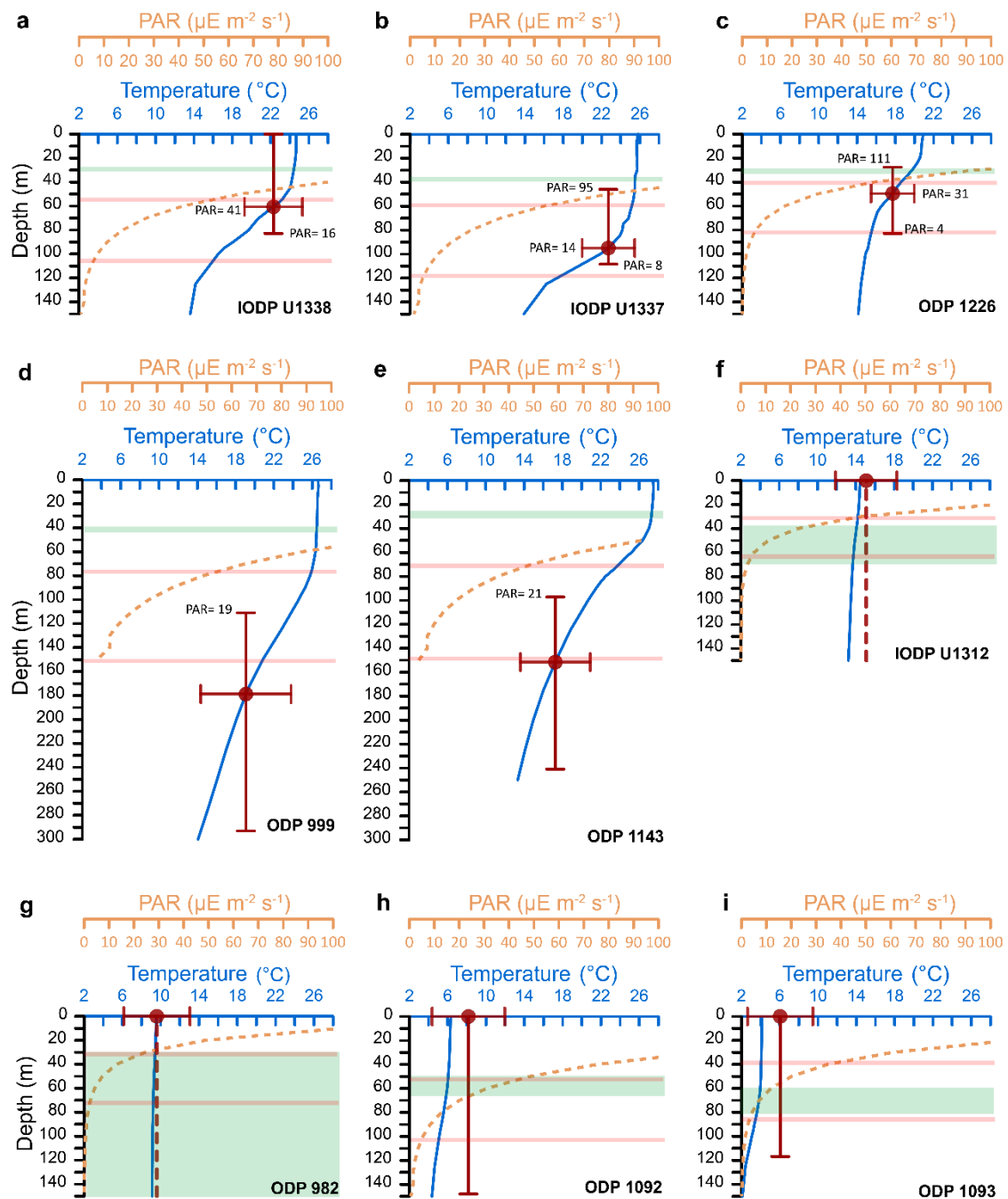
Fig. 4. Vertical temperature profile (solid blue line) and photosynthetic active radiation (PAR; dashed orange line) at our sites. Coccolith Δ_{47}-calcification temperatures (red circles) locate the likely habitat depth of coccolithophores. Horizontal error bars indicate the possible range of calcification temperature variation (95% CI). We use these warmest and coldest calcification temperatures to determine the potential shallowest and deepest habitat, respectively, here denoted by vertical error bars. Dashed vertical error bars indicate a potential habitat depth outside the depth scale in the y axis. The green shaded area indicates the variation of the base of the mixed layer during the peak production

553   months. Horizontal red lines comprise the depth where PAR varies between 10 and 1%

554   (limit of euphotic zone), below which coccolithophores are likely not living.

555

556   *4.2.2. High latitudes in the North and South Atlantic and the Southern Ocean*

557   At IODP Site U1312 and ODP Sites 982, 1092 and 1093, coccolith Δ_{47} calcification

558   temperatures agree within error with SSTs, suggesting a rather surficial production (Fig.

559   3, Fig. 4f-i). At higher latitudes, where the mixed layer is deeper than in low latitudes,

560   light availability is often more limited than nutrients (Dandonneau et al., 2004),

561   potentially forcing coccolithophores to remain closer to the surface. Given the relatively

562   large analytical uncertainty of clumped isotope thermometry, and the small vertical

563   temperature gradient typical of high latitudes, the attribution of a specific habitat depth in

564   these settings is less accurate compared to more stratified areas.

565   From the analysis of calcification temperatures and habitat depths of our tropical

566   locations, we conclude that PAR levels as low as 14 μE m^{-2} s^{-1} can sustain coccolithophore

567   production. Therefore, it is possible that high latitude coccolithophores can also thrive

568   under much lower than surface PAR levels (238-542 μE m^{-2} s^{-1} at our high latitude sites

569   during season of production). Requirement of rather low PAR levels for coccolithophore

570   production at high latitudes agree with the average mixed layer PAR levels (~1.5-12 E m^{-}

571   ^{2} d^{-1}, i.e. ~17-138 μE m^{-2} s^{-1}) reported for the Southern Ocean phytoplankton blooming

572   phase using extensive float data (Arteaga et al., 2020). Given the lack of motility during

573   their diploid phase, calcification of heterococcoliths in these sites is therefore likely

574   occurring throughout the mixed layer and not exclusively at the very surface. This

575   hypothesis also agrees with the larger overlap of irradiance levels in which lower photic

576   zone coccolithophore species from temperate zones are observed (Poulton et al., 2017).

577   Consequently, we suggest that coccolith Δ_{47} from well-mixed high latitudes are a good

578   indicator of mixed layer temperatures during the season of coccolithophore production.

579   Coccolith Δ_{47} temperatures at ODP Sites 1266 in the Walvis Ridge and 1122 in the

580   Pacific Sector of the Southern Ocean are 5.2 and 5.7 °C colder than SSTs during the

581   season of production, respectively. Such large differences, at places with a small

582   thermocline, result in unrealistic calculated habitat depth ranges, well below the euphotic

583   zone, where coccolithophores cannot photosynthesize (Fig. 4b, Supplementary Fig. J).

584   While ODP Site 1266 can be influenced by the Benguela upwelling system, especially

585   during winters, as filaments can extend up to 1000 km from the upwelling foci (Romero

586   et al., 2002), not even a total contribution of advected coccoliths from upwelling locations

587   can explain the cold Δ_{47} temperatures. With the available data, we cannot explain the

588   calcification temperature biases for these two Sites.

589   The North Atlantic highest latitude ODP Site 985, in contrast, show average coccolith

590   Δ_{47} temperatures 5.6 °C warmer than the season of production SSTs (Supplementary Fig.

591   J). This could be explained if, for instance, the preserved and analyzed coccoliths were

592   disproportionately produced during years with temperatures far warmer than those of the

593   modern ocean's season of production (e.g heat wave years).

594

595   **5. Implications for paleotemperature reconstructions**
596

597   If the commonly used temperature proxies all recorded surface ocean conditions, as is

598   commonly assumed, then they should also yield similar absolute values. In principle, this

599   assumption would be even more valid if proxies are phytoplankton-based, given their

600   light requirement for photosynthesis. If the habitat of placolith-bearing coccolithophores,

601   including alkenone producers, was invariably surficial geographically and temporally,

602    $U_{37}^{k\prime}$ and coccolith Δ_{47}-derived temperatures would be expected to show matching

603   absolute values corresponding to SSTs, since alkenones and coccolith $CaCO_3$ are both

604   produced by coccolithophores, and the $U_{37}^{k\prime}$ proxy is calibrated to SSTs (Müller et al.,

605   1998; Tierney and Tingley, 2018).

606   The comparison of $U_{37}^{k\prime}$ and coccolith Δ_{47} in the core tops shows that Δ_{47} calcification

607   temperatures estimated using Meinicke et al. (2021) are on average 4.7 °C colder than

608   SSTs recorded by the $U_{37}^{k\prime}$ proxy. One explanation is that coccolithophores are not

609   growing and calcifying at the surface in all oceanographic settings. In our dataset, $U_{37}^{k\prime}$-

610   derived temperatures are generally higher than measured SSTs during the season of

611   coccolithophore production (Fig. 3a, Supplementary Fig. F). On the other hand, Δ_{47}

612   calcification temperatures are colder than SSTs in tropical regions, which is consistent

613   with a deeper than surface production (Fig. 3b). This difference needs to be accounted for

614   in inter-proxy comparisons of coccolith Δ_{47} temperatures with proxies regressed to SST.

615

616   *5.1. Core top coccolith Δ_{47}-SST regression*
617

618   The most widely applied core top calibrations do not relate $U_{37}^{k\prime}$ to actual alkenone

619   production temperature, but rather to SST (Müller et al., 1998; Tierney and Tingley,

620   2018). We follow the same approach and calculate a core top coccolith Δ_{47}-SST

621   regression (Fig. 5a) to facilitate comparison of coccolith Δ_{47} calcification temperatures

622   with SST-regressed proxies like $U_{37}^{k\prime}$. The application of a York et al. (2004) regression

623   across all samples defines the following equation between coccolith Δ_{47} and average

624   WOA SSTs during peak production months:

625

626   Δ_{47} (I-CDES 90°C) = 0.0261 ± 0.0024 * $10^6/SST^2$ + 0.3198 ± 0.0280 (SST in K)   (1)
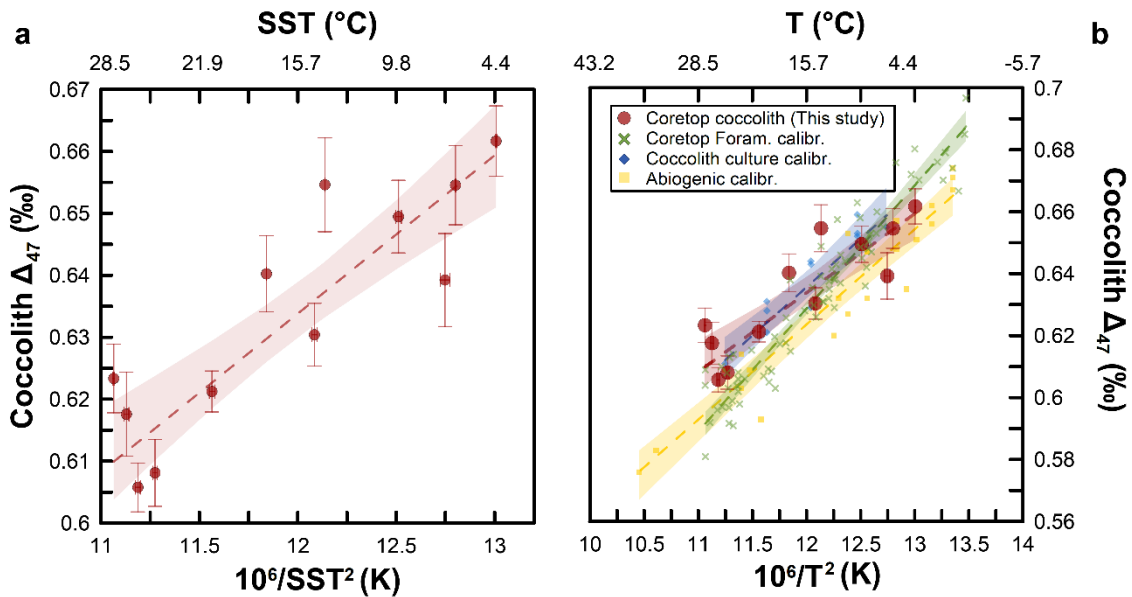
Fig. 5. a) Clumped isotopes (Δ_{47}, ‰) of our coccolith core top separations as a function of SST during the season of production, expressed both as $10^6/SST^2$ (SST in K), and as °C. Dashed red line represent the core top coccolith Δ_{47} regression, red shaded area represents the 95% CI. **b),** core top coccolith Δ_{47} regression (dashed red line, n=12) plotted together with the Anderson et al. (2021) (dashed yellow line, n=23), the Katz et al. (2017) (dashed blue line, n=11), and the Meinicke et al. (2021) calibrations (dashed green line, n=78), all obtained using the York et al. (2004) method. Shaded areas represent the 95% CI of the regressions. Vertical error bars represent 1SE of the Δ_{47} measurements, and horizontal error bars represent the average SE of the SSTs of the production months.

Our core top coccolith Δ_{47} show a strong and significant inverse correlation to average WOA SSTs (r = 0.8751; p< 0.001) (Fig 5a, Table 2). If coccolithophores were calcifying at depth rather than at the surface, a strong Δ_{47}-SST correlation can still arise because of the correlation between SSTs and temperatures at their habitat's depth.

Table 2. Regression of coccolith core top Δ_{47}-SST during season of production compared to recent Δ_{47} calibrations, including slope, intercept, and respective standard errors, all expressed in the I-CDES 90°C reference frame. The abiogenic (Anderson et al., 2021) and the coccolithophore culture (Katz et al., 2017) calibrations use experimental (Exp.) growth temperatures, while the planktonic foraminifera calibration (Coretop Foram) uses

28

648 inferred (Inf)/calculated *in situ* temperatures, not necessarily from the surface (Meinicke

649 et al., 2021). Standardization and data correction in the study of Katz et al. (2017) did not

650 follow the same methodology as applied for other studies, including ours, introducing

651 uncertainty in comparability between calibrations. Here we only consider data from the

652 Anderson et al. (2021) calibration in the range of temperature relevant for coccolithophore

653 environments (< 36.1 °C).

654

Regression (R)/Calibration (C)	Temp.	Slope±SE	Intercept±SE	r
R Coretop coccolith (this study)	SST	0.0261±0.0024	0.3198±0.0280	0.8751
C Coretop Foram. (Meinicke et al., 2021)	Inf. *in situ*	0.0397±0.0011	0.1518±0.0128	0.9174
C Culture (Katz et al., 2017)	Exp.	0.0313±0.0028	0.2602±0.0339	0.9410
C Abiogenic <36.1°C (Anderson et al., 2021)	Exp.	0.0307±0.0035	0.2549±0.0422	0.9521

655

656 ANCOVA analyses show that the slope and the intercept of our coccolith Δ_{47}

657 regression are not statistically different from those of Anderson et al. (2021) ($p_{slope} = 0.11$;

658 $p_{intercept} = 0.08$; data <40 °C), while they are different to the those of the foraminifera

659 calibration (Meinicke et al., 2021; $p_{slope} < 0.005$; $p_{intercept} < 0.005$) (Supplementary Table

660 E). Even if not statistically different to the abiotic calibration, the slope of the coccolith

661 Δ_{47}-SST regression is shallower compared to the theoretical value and all mentioned Δ_{47}

662 calibrations (Fig. 5b; Table 2). This shallower slope is especially influenced by a few

663 warm samples, thus supporting the notion that especially at tropical sites coccoliths have

664 deeper and cooler habitats. This can explain the larger offset between SST and Δ_{47}

665 calcification temperatures at lower warmer latitudes than at colder higher ones. A

666 shallower slope and a slight mismatch between our coccolith Δ_{47}-SST regression and

667 other published Δ_{47} calibrations would be a further argument for a deeper than surface

668 coccolith calcification in some ocean settings, as temperatures from other calibrations are

669 either experimental or inferred *in situ*. Conversely, our regression uses SSTs, regardless

670 if they match or not actual calcification temperatures.

Because the coccolith Δ_{47}-SST regression does not account for the potential for calcification at depth, we emphasize that it should be not used to calculate SSTs. It could be rather used as a tool to compare to SST-regressed proxies (like $U^{k'}_{37}$) in future studies, taking into account that this approach would lead to overestimation of absolute temperatures of production. Further work on both proxies is required to improve absolute temperature reconstructions and resolve the implication of production depth on estimation of SST.
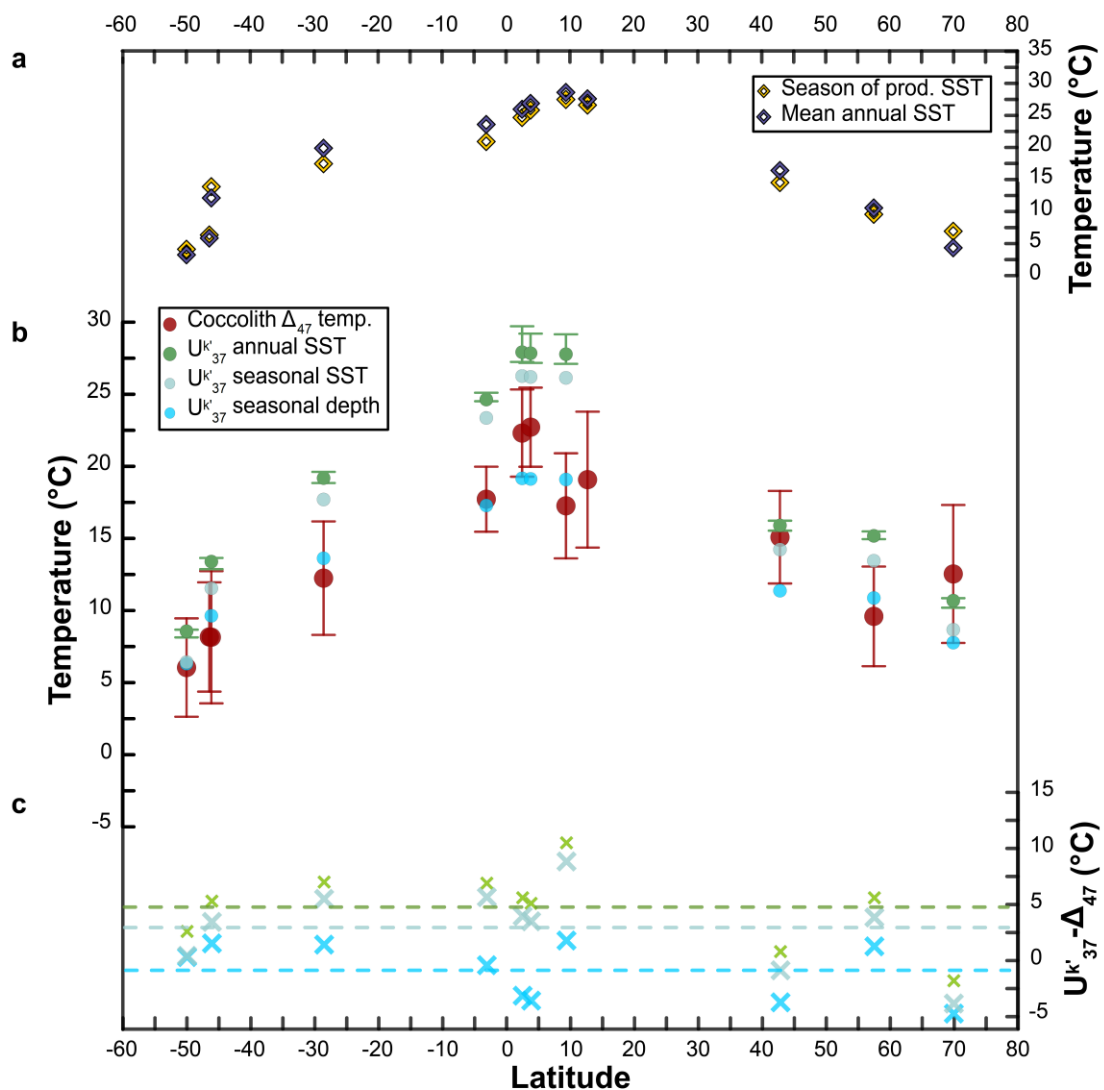
Fig. 6. a) Mean annual SSTs (deep blue diamonds) and SSTs during peak production months (yellow diamonds). **b)** Calcification temperatures (±95% CI) from coccolith Δ_{47} calculated with the foraminifera calibration (Meinicke et al., 2021) (red circles); mean

682   annual SSTs (green circles) applying published (Müller et al., 1998; Prahl et al., 1988;

683   Tierney and Tingley, 2018) $U_{37}^{k\prime}$ calibrations to our $U_{37}^{k\prime}$; seasonal SSTs (blue-green

684   circles) applying an independent $U_{37}^{k\prime}$-seasonal SST regression to our $U_{37}^{k\prime}$, which is based

685   on a subset of sites of the study of Tierney and Tingley (2018), which coincide

686   geographically with our locations; and seasonal temperatures at depth of production (light

687   blue circles) applying an independent $U_{37}^{k\prime}$-seasonal depth temperature regression to our

688    $U_{37}^{k\prime}$, based on the same subset of sites from Tierney and Tingley (2018), and considering

689   habitat depths inferred from our coccolith Δ_{47} database. **c)** Difference between $U_{37}^{k\prime}$-

690   annual SSTs (green cross, average difference 4.7 °C), $U_{37}^{k\prime}$ seasonal SSTs (blue-green

691   crosses, average difference 3.0 °C), and $U_{37}^{k\prime}$ seasonal deep temperatures (light blue

692   crosses, average difference -0.9 °C) and coccolith Δ_{47}-calcification temperatures

693   (Meinicke et al., 2021).

694

695   *5.2. Snapshot into alternative alkenone calibrations: are alkenones also produced at depth?*
696

697   We compare the relationship between $U_{37}^{k\prime}$ and seasonal SSTs (rather than annual) and

698   to subsurface temperatures. For this, we selected an independent sample set, a subset of

699   sites from the alkenone calibration work of Tierney and Tingley (2018), which are

700   proximal to our sites and for which we apply similar season and habitat of production.

701   For this independent sample subset, we then calculated alternative $U_{37}^{k\prime}$ calibrations using:

702   a) SSTs during the season of production, and b) temperatures at the depth and season of

703   production inferred for that oceanic setting from our coccolith Δ_{47} dataset (Fig. 6 d, e,

704   Supplementary Note E and Fig. K). We propose that alternative $U_{37}^{k\prime}$ calibrations

705   considering seasonal temperatures of calcification and alkenone production at depth with

706   a large $U_{37}^{k\prime}$ dataset could improve the robustness and coherency of paleotemperature

707   estimates.

708

6. Conclusions

Coccoliths from globally distributed core top sediments show promise for Δ_{47} thermometry, since Δ_{47} correlates with sea surface temperatures during the production season and also correlates with the temperature component of $\delta^{18}O$ variation in coccoliths ($\delta^{18}O_{calcite}$- $\delta^{18}O_w$). Application of the statistically-robust and carbonate-standardized foraminifera Δ_{47} calibration, the most appropriate available calibration for biogenic carbonate, yields coccolith calcification temperatures colder than SSTs for all tropical locations. This suggests that coccolithophores at these locations likely live at depth and can thrive with PAR levels between 1-10%. For well-mixed high latitudes, coccolith Δ_{47} calcification temperatures likely reflect mixed layer temperatures.

Because phytoplankton's ability to accumulate cells in the ocean depends on a complex conjunction of forcing factors, their actual habitat may not obey the convenient simplifications historically used for calibration of their temperature proxies. Future studies will determine if the use of a statistically well-constrained coccolith Δ_{47} calibration could further reduce uncertainties in estimated absolute calcification temperatures and habitat depths. Potentially, coccolith Δ_{47} combined with concurrent analysis of planktic foraminifera occupying different depths, could be used to add constraints on the vertical thermal structure of the photic zone.

If further work substantiates the evidence here for significant deep photic zone production by alkenone-producing coccolithophores in some (or all) oceanic settings, the convention of regressing the $U_{37}^{k'}$ parameter to surface ocean temperature may need reassessment to account for the spatially (and potentially temporally) variable relationship between production and surface temperatures. The assignment of absolute temperatures to their correct depth would allow climate models to compare their outputs with more accurate datasets, improving their reliability.

735

Author contributions

L.M.M and H.Z developed the separation method; A.F developed the cleaning method; L.M.M separated and cleaned the coccoliths, and with M.J measured clumped isotopes under the direction of S.B; L.M.M and M.J prepared and measured samples for trace element analysis. L.M.M took the SEM pictures; H.Z. evaluated coccolith assemblages. L.M.M purified alkenones and L.M.M and J.G. measured alkenones. I.H.A helped with data acquisition. N.H measured radiocarbon. The study was conceived by L.M.M, H.S and S.B. L.M.M wrote the paper with contributions from H.S and S.B.

Declaration of competing interests

There are no competing interests.

Additional information

Supplementary information is available in the online version of the paper.

758

759 **References**

760 Agterhuis, T., Ziegler, M., de Winter, N.J., Lourens, L.J., 2022. Warm deep-sea
761   temperatures across Eocene Thermal Maximum 2 from clumped isotope
762   thermometry. Communications Earth & Environment 2022 3:1 3, 1–9.
763   https://doi.org/10.1038/s43247-022-00350-8
764 Anderson, N.T., Kelson, J.R., Kele, S., Daëron, M., Bonifacie, M., Horita, J., Mackey,
765   T.J., John, C.M., Kluge, T., Petschnig, P., Jost, A.B., Huntington, K.W.,
766   Bernasconi, S.M., Bergmann, K.D., 2021. A Unified Clumped Isotope
767   Thermometer Calibration (0.5–1,100°C) Using Carbonate-Based Standardization.
768   Geophys Res Lett 48, e2020GL092069. https://doi.org/10.1029/2020GL092069
769 Arteaga, L.A., Boss, E., Behrenfeld, M.J., Westberry, T.K., Sarmiento, J.L., 2020.
770   Seasonal modulation of phytoplankton biomass in the Southern Ocean. Nature
771   Communications 2020 11:1 11, 1–10. https://doi.org/10.1038/s41467-020-19157-2
772 Balch, W.M., Bowler, B.C., Drapeau, D.T., Lubelczyk, L.C., Lyczkowski, E., Mitchell,
773   C., Wyeth, A., 2019. Coccolithophore distributions of the North and South Atlantic
774   Ocean. Deep Sea Research Part I: Oceanographic Research Papers 151, 103066.
775   https://doi.org/10.1016/J.DSR.2019.06.012
776 Beaufort, L., Couapel, M., Buchet, N., Claustre, H., Goyet, C., 2008. Calcite production
777   by coccolithophores in the south east Pacific Ocean. Biogeosciences 5, 1101–1117.
778   https://doi.org/10.5194/bg-5-1101-2008
779 Behrenfeld, M.J., Doney, S.C., Lima, I., Boss, E.S., Siegel, D.A., 2013. Annual cycles
780   of ecological disturbance and recovery underlying the subarctic Atlantic spring
781   plankton bloom. Global Biogeochem Cycles 27, 526–540.
782   https://doi.org/10.1002/gbc.20050
783 Bernasconi, S.M., Daëron, M., Bergmann, K.D., Bonifacie, M., Meckler, A.N., Affek,
784   H.P., Anderson, N., Bajnai, D., Barkan, E., Beverly, E., Blamart, D., Burgener, L.,
785   Calmels, D., Chaduteau, C., Clog, M., Davidheiser-Kroll, B., Davies, A., Dux, F.,
786   Eiler, J., Elliott, B., Fetrow, A.C., Fiebig, J., Goldberg, S., Hermoso, M.,
787   Huntington, K.W., Hyland, E., Ingalls, M., Jaggi, M., John, C.M., Jost, A.B., Katz,
788   S., Kelson, J., Kluge, T., Kocken, I.J., Laskar, A., Leutert, T.J., Liang, D.,
789   Lucarelli, J., Mackey, T.J., Mangenot, X., Meinicke, N., Modestou, S.E., Müller,
790   I.A., Murray, S., Neary, A., Packard, N., Passey, B.H., Pelletier, E., Petersen, S.,
791   Piasecki, A., Schauer, A., Snell, K.E., Swart, P.K., Tripati, A., Upadhyay, D.,
792   Vennemann, T., Winkelstern, I., Yarian, D., Yoshida, N., Zhang, N., Ziegler, M.,
793   2021. InterCarb: A Community Effort to Improve Interlaboratory Standardization
794   of the Carbonate Clumped Isotope Thermometer Using Carbonate Standards.
795   Geochemistry, Geophysics, Geosystems 22, e2020GC009588.
796   https://doi.org/10.1029/2020GC009588
797 Bouchard', J.N., Roy, S., Campbell', D.A., 2006. UVB Effects on the Photosystem II-
798   D1 Protein of Phytoplankton and Natural Phytoplankton Communities. Photochem
799   Photobiol 82, 936–951. https://doi.org/10.1562/2005-08-31-IR-666
800 Caldarescu, D.E., Sadatzki, H., Andersson, C., Schäfer, P., Fortunato, H., Meckler,
801   A.N., 2021. Clumped isotope thermometry in bivalve shells: A tool for
802   reconstructing seasonal upwelling. Geochim Cosmochim Acta 294, 174–191.
803   https://doi.org/10.1016/J.GCA.2020.11.019
804 Cortés, M.Y., Bollmann, J., Thierstein, H.R., 2001. Coccolithophore ecology at the
805   HOT station ALOHA, Hawaii. Deep Sea Res 2 Top Stud Oceanogr 48, 1957–
806   1981. https://doi.org/10.1016/S0967-0645(00)00165-X

807   Dandonneau, Y., Deschamps, P.Y., Nicolas, J.M., Loisel, H., Blanchot, J., Montel, Y.,
808   Thieuleux, F., Bécu, G., 2004. Seasonal and interannual variability of ocean color
809   and composition of phytoplankton communities in the North Atlantic, equatorial
810   Pacific and South Pacific. Deep Sea Research Part II: Topical Studies in
811   Oceanography 51, 303–318. https://doi.org/10.1016/J.DSR2.2003.07.018
812   Drury, A.J., John, C.M., 2016. Exploring the potential of clumped isotope thermometry
813   on coccolith-rich sediments as a sea surface temperature proxy. Geochemistry,
814   Geophysics, Geosystems 17, 4092–4104. https://doi.org/10.1002/2016GC006459
815   Dudley, W.C., Blackwelder, P., Brand, L., Duplessy, J.C., 1986. Stable isotopic
816   composition of coccoliths. Mar Micropaleontol 10, 1–8.
817   https://doi.org/10.1016/0377-8398(86)90021-6
818   Eide, M., Olsen, A., Ninnemann, U.S., Johannessen, T., 2017. A global ocean
819   climatology of preindustrial and modern ocean $\delta^{13}C$. Global Biogeochem Cycles
820   31, 515–534. https://doi.org/10.1002/2016GB005473
821   Eiler, J.M., 2011. Paleoclimate reconstruction using carbonate clumped isotope
822   thermometry. Quat Sci Rev 30, 3575–3588.
823   https://doi.org/10.1016/j.quascirev.2011.09.001
824   Eiler, J.M., 2007. "Clumped-isotope" geochemistry-The study of naturally-occurring,
825   multiply-substituted isotopologues. Earth Planet Sci Lett 262, 309–327.
826   https://doi.org/10.1016/j.epsl.2007.08.020
827   Evans, D., Sagoo, N., Renema, W., Cotton, L.J., Müller, W., Todd, J.A., Saraswati,
828   P.K., Stassen, P., Ziegler, M., Pearson, P.N., Valdes, P.J., Affek, H.P., 2018.
829   Eocene greenhouse climate revealed by coupled clumped isotope-Mg/Ca
830   thermometry. Proc Natl Acad Sci U S A 115, 1174–1179.
831   https://doi.org/10.1073/PNAS.1714744115/SUPPL_FILE/PNAS.1714744115.SD0
832   2.XLSX
833   Fernandez, A., Müller, I.A., Rodríguez-Sanz, L., Dijk, J. van, Looser, N., Bernasconi,
834   S.M., 2017. A Reassessment of the Precision of Carbonate Clumped Isotope
835   Measurements: Implications for Calibrations and Paleoclimate Reconstructions.
836   Geochemistry, Geophysics, Geosystems 18, 4375–4386.
837   https://doi.org/10.1002/2017GC007106@10.1002/(ISSN)1525-2027.ISOTOPE1
838   Fiebig, J., Daëron, M., Bernecker, M., Guo, W., Schneider, G., Boch, R., Bernasconi,
839   S.M., Jautzy, J., Dietzel, M., 2021. Calibration of the dual clumped isotope
840   thermometer for carbonates. Geochim Cosmochim Acta 312, 235–256.
841   https://doi.org/10.1016/J.GCA.2021.07.012
842   Ghosh, P., Adkins, J., Affek, H., Balta, B., Guo, W., Schauble, E.A., Schrag, D., Eiler,
843   J.M., 2006. 13C-18O bonds in carbonate minerals: A new kind of
844   paleothermometer. Geochim Cosmochim Acta 70, 1439–1456.
845   https://doi.org/10.1016/j.gca.2005.11.014
846   Guan, W., Gao, K., 2010. Impacts of UV radiation on photosynthesis and growth of the
847   coccolithophore Emiliania huxleyi (Haptophyceae). Environ Exp Bot 67, 502–508.
848   https://doi.org/10.1016/J.ENVEXPBOT.2009.08.003
849   Guitián, J., Stoll, H.M., 2021. Evolution of Sea Surface Temperature in the Southern
850   Mid-latitudes From Late Oligocene Through Early Miocene. Paleoceanogr
851   Paleoclimatol 36, e2020PA004199. https://doi.org/10.1029/2020PA004199
852   Hermoso, M., Candelier, Y., Browning, T.J., Minoletti, F., 2015. Environmental control
853   of the isotopic composition of subfossil coccolith calcite: Are laboratory culture
854   data transferable to the natural environment? GeoResJ 7, 35–42.
855   https://doi.org/10.1016/J.GRJ.2015.05.002

Hermoso, M., Horner, T.J., Minoletti, F., Rickaby, R.E.M., 2014. Constraints on the vital effect in coccolithophore and dinoflagellate calcite by oxygen isotopic modification of seawater. Geochim Cosmochim Acta 141, 612–627. https://doi.org/10.1016/J.GCA.2014.05.002

Ho, S.L., Laepple, T., 2016. Flat meridional temperature gradient in the early Eocene in the subsurface rather than surface ocean. Nat Geosci 9, 606–610. https://doi.org/10.1038/ngeo2763

John, C.M., Bowen, D., 2016. Community software for challenging isotope analysis: First applications of 'Easotope' to clumped isotopes. Rapid Communications in Mass Spectrometry 30, 2285–2300. https://doi.org/10.1002/rcm.7720

Katz, A., Bonifacie, M., Hermoso, M., Cartigny, P., Calmels, D., 2017. Laboratory-grown coccoliths exhibit no vital effect in clumped isotope ($\Delta 47$) composition on a range of geologically relevant temperatures. Geochim Cosmochim Acta 208, 335–353. https://doi.org/10.1016/j.gca.2017.02.025

Kretschmer, K., Jonkers, L., Kucera, M., Schulz, M., 2018. Modeling seasonal and vertical habitats of planktonic foraminifera on a global scale. Biogeosciences 15, 4405–4429. https://doi.org/10.5194/BG-15-4405-2018

LeGrande, A.N., Schmidt, G.A., 2006. Global gridded data set of the oxygen isotopic composition in seawater. Geophys Res Lett 33, 12604. https://doi.org/10.1029/2006GL026011

Leutert, T.J., Auderset, A., Martínez-García, A., Modestou, S., Meckler, A.N., 2020. Coupled Southern Ocean cooling and Antarctic ice sheet expansion during the middle Miocene. Nature Geoscience 2020 13:9 13, 634–639. https://doi.org/10.1038/s41561-020-0623-0

Leutert, T.J., Modestou, S., Bernasconi, S.M., Meckler, A.N., 2021. Southern ocean bottom-water cooling and ice sheet expansion during the middle Miocene climate transition. Climate of the Past 17, 2255–2271. https://doi.org/10.5194/CP-17-2255-2021

Liu, H., Wang, D., Yun, M., Zhang, X., Zhang, G., Thangaraj, S., Sun, J., 2021. Vertical Biogeography and Realized Niche Traits of Living Coccolithophore Community in the Eastern Indian Ocean. J Geophys Res Biogeosci 126, e2020JG005922. https://doi.org/10.1029/2020JG005922

Lunt, D.J., Bragg, F., Chan, W. le, Hutchinson, D.K., Ladant, J.B., Morozova, P., Niezgodzki, I., Steinig, S., Zhang, Z., Zhu, J., Abe-Ouchi, A., Anagnostou, E., de Boer, A.M., Coxall, H.K., Donnadieu, Y., Foster, G., Inglis, G.N., Knorr, G., Langebroek, P.M., Lear, C.H., Lohmann, G., Poulsen, C.J., Sepulchre, P., Tierney, J.E., Valdes, P.J., Volodin, E.M., Dunkley Jones, T., Hollis, C.J., Huber, M., Otto-Bliesner, B.L., 2021. DeepMIP: Model intercomparison of early Eocene climatic optimum (EECO) large-scale climate features and comparison with proxy data. Climate of the Past 17, 203–227. https://doi.org/10.5194/CP-17-203-2021

McIntyre, C.P., Wacker, L., Haghipour, N., Blattmann, T.M., Fahrni, S., Usman, M., Eglinton, T.I., Synal, H.A., 2017. Online 13C and 14C Gas Measurements by EA-IRMS–AMS at ETH Zürich. Radiocarbon 59, 893–903. https://doi.org/10.1017/RDC.2016.68

Meckler, A.N., Sexton, P.F., Piasecki, A.M., Leutert, T.J., Marquardt, J., Ziegler, M., Agterhuis, T., Lourens, L.J., Rae, J.W.B., Barnet, J., Tripati, A., Bernasconi, S.M., 2022. Cenozoic evolution of deep ocean temperature from clumped isotope thermometry. Science (1979) 377, 86–90. https://doi.org/10.1126/SCIENCE.ABK0604/SUPPL_FILE/SCIENCE.ABK0604_DATA_S1_TO_S3.ZIP

906 Meinicke, N., Ho, S.L., Hannisdal, B., Nürnberg, D., Tripati, A., Schiebel, R., Meckler,
907   A.N., 2020. A robust calibration of the clumped isotopes to temperature
908   relationship for foraminifers. Geochim Cosmochim Acta 270, 160–183.
909   https://doi.org/10.1016/J.GCA.2019.11.022
910 Meinicke, N., Reimi, M.A., Ravelo, A.C., Meckler, A.N., 2021. Coupled Mg/Ca and
911   Clumped Isotope Measurements Indicate Lack of Substantial Mixed Layer Cooling
912   in the Western Pacific Warm Pool During the Last ~5 Million Years. Paleoceanogr
913   Paleoclimatol 36, e2020PA004115. https://doi.org/10.1029/2020PA004115
914 Mejía, L.M., Ziveri, P., Cagnetti, M., Bolton, C., Zahn, R., Marino, G., Martínez-
915   Méndez, G., Stoll, H., 2014. Effects of midlatitude westerlies on the
916   paleoproductivity at the Agulhas Bank slope during the penultimate glacial cycle:
917   Evidence from coccolith Sr/Ca ratios. Paleoceanography 29.
918   https://doi.org/10.1002/2013PA002589
919 Mignot, A., Ferrari, R., Claustre, H., 2018. Floats with bio-optical sensors reveal what
920   processes trigger the North Atlantic bloom. Nat Commun 9, 1–9.
921   https://doi.org/10.1038/s41467-017-02143-6
922 Müller, I.A., Rodriguez-Blanco, J.D., Storck, J.C., do Nascimento, G.S., Bontognali,
923   T.R.R., Vasconcelos, C., Benning, L.G., Bernasconi, S.M., 2019. Calibration of the
924   oxygen and clumped isotope thermometers for (proto-)dolomite based on synthetic
925   and natural carbonates. Chem Geol 525, 1–17.
926   https://doi.org/10.1016/J.CHEMGEO.2019.07.014
927 Müller, P.J., Kirst, G., Ruhland, G., von Storch, I., Rosell-Melé, A., 1998. Calibration
928   of the alkenone paleotemperature index UK'37 based on core-tops from the eastern
929   South Atlantic and the global ocean (60°N-60°S). Geochim Cosmochim Acta 62,
930   1757–1772. https://doi.org/10.1016/S0016-7037(98)00097-0
931 Peral, M., Bassinot, F., Daëron, M., Blamart, D., Bonnin, J., Jorissen, F., Kissel, C.,
932   Michel, E., Waelbroeck, C., Rebaubier, H., Gray W. R, 2022. On the combination
933   of the planktonic foraminiferal Mg/Ca, clumped (Δ47) and conventional (δ18O)
934   stable isotope paleothermometers in palaeoceanographic studies. Geochim
935   Cosmochim Acta Preprint. https://doi.org/https://doi.org/10.31223/X5VK82
936 Peral, M., Daëron, M., Blamart, D., Bassinot, F., Dewilde, F., Smialkowski, N., Isguder,
937   G., Bonnin, J., Jorissen, F., Kissel, C., Michel, E., Vázquez Riveiros, N.,
938   Waelbroeck, C., 2018. Updated calibration of the clumped isotope thermometer in
939   planktonic and benthic foraminifera. Geochim Cosmochim Acta 239, 1–16.
940   https://doi.org/10.1016/j.gca.2018.07.016
941 Piasecki, A., Bernasconi, S.M., Grauel, A., Hannisdal, B., Ho, S.L., Leutert, T.J.,
942   Marchitto, T.M., Meinicke, N., Tisserand, A., Meckler, N., 2019. Application of
943   clumped isotope thermometry to benthic foraminifera. Geochemistry, Geophysics,
944   Geosystems 20, 2082–2090. https://doi.org/10.1029/2018GC007961
945 Poulton, A.J., Holligan, P.M., Charalampopoulou, A., Adey, T.R., 2017.
946   Coccolithophore ecology in the tropical and subtropical Atlantic Ocean: New
947   perspectives from the Atlantic meridional transect (AMT) programme. Prog
948   Oceanogr 158, 150–170. https://doi.org/10.1016/J.POCEAN.2017.01.003
949 Prahl, F.G., Muehlhausen, L.A., Zahnle, D.L., 1988. Further evaluation of long-chain
950   alkenones as indicators of paleoceanographic conditions. Geochim Cosmochim
951   Acta 52, 2303–2310. https://doi.org/10.1016/0016-7037(88)90132-9
952 Rebotim, A., Voelker, A.H.L., Jonkers, L., Waniek, J.J., Meggers, H., Schiebel, R.,
953   Fraile, I., Schulz, M., Kucera, M., 2017. Factors controlling the depth habitat of
954   planktonic foraminifera in the subtropical eastern North Atlantic. Biogeosciences
955   14, 827–859. https://doi.org/10.5194/bg-14-827-2017

956 Richter, F.M., Liang, Y., 1993. The rate and consequences of Sr diagenesis in deep-sea
957   carbonates. Earth Planet Sci Lett 117, 553–565. https://doi.org/10.1016/0012-
958   821X(93)90102-F
959 Rodríguez-Sanz, L., Bernasconi, S.M., Marino, G., Heslop, D., Müller, I.A., Fernandez,
960   A., Grant, K.M., Rohling, E.J., 2017. Penultimate deglacial warming across the
961   Mediterranean Sea revealed by clumped isotopes in foraminifera. Scientific
962   Reports 2017 7:1 7, 1–11. https://doi.org/10.1038/s41598-017-16528-6
963 Romero, O., Boeckel, B., Donner, B., Lavik, G., Fischer, G., Wefer, G., 2002. Seasonal
964   productivity dynamics in the pelagic central Benguela System inferred from the
965   flux of carbonate and silicate organisms. Journal of Marine Systems 37, 259–278.
966   https://doi.org/10.1016/S0924-7963(02)00189-6
967 Rommerskirchen, F., Condon, T., Mollenhauer, G., Dupont, L., Schefuss, E., 2011.
968   Miocene to Pliocene development of surface and subsurface temperatures in the
969   Benguela Current system. Paleoceanography 26.
970   https://doi.org/10.1029/2010PA002074
971 Schauble, E.A., Ghosh, P., Eiler, J.M., 2006. Preferential formation of 13C-18O bonds
972   in carbonate minerals, estimated using first-principles lattice dynamics. Geochim
973   Cosmochim Acta 70, 2510–2529. https://doi.org/10.1016/j.gca.2006.02.011
974 Schlitzer, R., 2021. Ocean Data View, odv.awi.de.
975 Schouten, S., Hopmans, E.C., Sinninghe Damsté, J.S., 2013. The organic geochemistry
976   of glycerol dialkyl glycerol tetraether lipids: A review. Org Geochem 54, 19–61.
977   https://doi.org/10.1016/j.orggeochem.2012.09.006
978 Spero, H.J., Mielke, K.M., Kalve, E.M., Lea, D.W., Pak, D.K., 2003. Multispecies
979   approach to reconstructing eastern equatorial Pacific thermocline hydrography
980   during the past 360 kyr. Paleoceanography 18, 1022.
981   https://doi.org/10.1029/2002PA000814
982 Spooner, P.T., Guo, W., Robinson, L.F., Thiagarajan, N., Hendry, K.R., Rosenheim,
983   B.E., Leng, M.J., 2016. Clumped isotope composition of cold-water corals: A role
984   for vital effects? Geochim Cosmochim Acta 179, 123–141.
985   https://doi.org/10.1016/J.GCA.2016.01.023
986 Tagliavento, M., John, C.M., Stemmerik, L., 2019. Tropical temperature in the
987   Maastrichtian Danish Basin: Data from coccolith Δ47 and δ18O. Geology 47,
988   1074–1078. https://doi.org/10.1130/G46671.1
989 Tierney, J.E., Sinninghe Damsté, J.S., Pancost, R.D., Sluijs, A., Zachos, J.C., 2017a.
990   Eocene temperature gradients. Nat Geosci 10, 538–539.
991   https://doi.org/10.1038/ngeo2997
992 Tierney, J.E., Tingley, M.P., 2018. BAYSPLINE: A New Calibration for the Alkenone
993   Paleothermometer. Paleoceanogr Paleoclimatol 33, 281–301.
994   https://doi.org/10.1002/2017PA003201
995 Tripati, A.K., Eagle, R.A., Thiagarajan, N., Gagnon, A.C., Bauch, H., Halloran, P.R.,
996   Eiler, J.M., 2010. 13C-18O isotope signatures and "clumped isotope" thermometry
997   in foraminifera and coccoliths. Geochim Cosmochim Acta 74, 5697–5717.
998   https://doi.org/10.1016/j.gca.2010.07.006
999 WOA, 2018. World Ocean Atlas 2018 Data Access [WWW Document]. URL
1000   https://www.ncei.noaa.gov/access/world-ocean-atlas-2018/ (accessed 4.4.22).
1001 York, D., Evensen, N., López-Martínez, M., de Basabe Delgado, J., 2004. Unified
1002   equations for the slope, intercept, and standard errors of the best straight line. Am J
1003   Phys 72. https://doi.org/10.1119/1.1632486

1004 Zhang, H., Liu, C., Mejía, L.M., Stoll, H., 2021. Technical note: Accelerate coccolith
1005   size separation via repeated centrifugation. Biogeosciences 18, 1909–1916.
1006   https://doi.org/10.5194/BG-18-1909-2021
1007 Zhu, J., Poulsen, C.J., Tierney, J.E., 2019. Simulation of Eocene extreme warmth and
1008   high climate sensitivity through cloud feedbacks. Sci Adv 5.
1009   https://doi.org/10.1126/SCIADV.AAX1874/SUPPL_FILE/AAX1874_TABLES_S
1010   1_AND_S2.XLSX
1011 Ziveri, P., Stoll, H., Probert, I., Klaas, C., Geisen, M., Ganssen, G., Young, J., 2003.
1012   Stable isotope 'vital effects' in coccolith calcite. Earth Planet Sci Lett 210, 137–
1013   149. https://doi.org/10.1016/S0012-821X(03)00101-8
1014

Clumped isotope temperatures applied to Holocene coccoliths reveal their habitat depth

Luz María Mejía, Stefano M. Bernasconi, Hongrui Zhang, José Guitián, Alvaro Fernandez, Ivan Hernández-Almeida, Madalina Jaggi, Negar Haghipour, Heather Stoll

Supplementary Table A. Sample details (leg, site, core, type, section and interval) for our core top locations.

Leg/Exp	Site	Hole	Core	Type	Section	Interval (cm)	
						Top	Bottom
177	1093	A	1	H	2	6	8
177	1092	C	1	H	1	8	10
181	1122	C	1	H	1	31	33
208	1266	B	1	H	1	3.5	5
201	1226	C	1	H	1	14	16
321	U1338	A	1	H	1	0	2
321	U1337	B	1	H	1	8	10
184	1143	A	1	H	1	22	24
165	999	A	1	H	1	0	2
306	U1312	B	1	H	1	15	17
162	982	B	1	H	1	35	37
162	985	B	1	H	1	12	14

Supplementary Table B. Radiocarbon ages (y) for all locations analyzed, showing our core top samples are mid to late Holocene.

Site	$F^{14}C$	age (y)
1093	0.3953 ± 0.0074	7456 ± 150
1092	0.4787 ± 0.0043	5918 ± 72
1122	0.5039 ± 0.0044	5506 ± 69
1266	0.6153 ± 0.0048	3901 ± 63
1226	0.6870 ± 0.0052	3016 ± 61
U1338	0.5195 ± 0.0050	5261 ± 77
U1337	0.3384 ± 0.0042	8704 ± 100
1143	$0.611 0\pm 0.0051$	3958 ± 67
999	0.6575 ± 0.0050	3368 ± 61
U1312	0.4456 ± 0.0044	6493 ± 79
982	0.4401 ± 0.0056	6593 ± 103
985	0.5931 ± 0.0054	4196 ± 73

13 **Supplementary Table C.** $\delta^{13}C$ (VPDV), $\delta^{18}O$ (VPDV), Δ_{47} (CDES) and Δ_{47} temperatures from the standard
14 ETH 3 before and after accelerated solvent extraction, and from a sample from ODP Site 1266 at the Walvis
15 Ridge before and after H_2O_2 oxidation. Standard errors are shown for $\delta^{13}C$, $\delta^{18}O$ and Δ_{47} values, and 95%
16 confidence interval is shown for the Δ_{47}–derived temperatures.

17

	$\delta^{13}C\pm SD$ (‰)	$\delta^{18}O\pm SD$ (‰)	$\Delta_{47}\pm SD$ (‰)	n	Δ_{47} temp$\pm$CI (95%) (°C)
ETH 3 pre ASE	1.69±0.01	-1.74±0.03	0.6087±0.016	10	21.8±4.10
ETH 3 post ASE	1.69±0.01	-1.73±0.03	0.6198±0.019	11	18.30±3.80
1266 pre oxidized	0.38±0.05	0.04±0.05	0.6521±0.027	13	8.86±4.65
1266 post oxidized	0.43±0.06	0.08±0.05	0.6493±0.019	11	9.50±3.65

18

19

20 **Supplementary Note A. Negligible cold biases from diagenetic processes**

21   The colder than SSTs calcification temperatures derived from coccolith Δ_{47} of some of our locations are
22 not a consequence of diagenetic processes. This was confirmed by SEM observation of non-fragmented
23 coccoliths (Supplementary Fig. A) and trace element analysis of our young samples (< 8700 y). When there
24 is a significant contribution of authigenic carbonate, which is produced at the seafloor and therefore colder
25 temperatures compared to the surface water coccolith signal, a cold bias is introduced (Eiler, 2007).
26 Although SEM analysis does show partial dissolution of coccoliths in some samples, it does not suggest
27 overgrowth of abiogenic carbonate in the bottom ocean (Supplementary Fig. A). Most of the coccolith
28 separations analyzed for Δ_{47} in this study include the <2 µm size fraction, since removing it highly increases
29 separation time and effort. Even though SEM techniques do not allow to recognize authigenic carbonate in
30 this size fraction, the negligible contribution of authigenic carbonate is supported by the Sr/Ca ratios of our
31 separations, with values (1.98-2.61 mmol/mol) (Supplementary Table D) that are consistent with
32 estimations from coccolithophore cultures, sediment traps and downcore sediments (Mejía et al., 2014 and
33 refs, therein), and which are higher than values expected from calcite precipitated from seawater or pore
34 fluids (Richter and Liang, 1993). Mg and Al can also be indicative of diagenetic processes, the presence of
35 dolomitic calcite or clay content. The Mg/Ca ratio can increase when detrital dolomite or high Mg/Ca
36 phases are present, but can also be high in samples of low $CaCO_3$ content due to the increased significance
37 of Mg in clays. Indeed Mg/Ca is high in clay-rich samples of high Al/Ca. The Mg/Al ratio is therefore used
38 as an indicator of the significance of detrital Mg-rich $CaCO_3$. Similar Mg/Al ratios suggest that our samples
39 do not feature large variations in the relative abundance of high Mg $CaCO_3$ from diagenetic or detrital
40 sources (Supplementary Table D).

41

42

43

Supplementary Table D. Trace element analysis (Sr/Ca, Mg/Ca, Al/Ca, Mg/Al) of the coccolith core top separations. Sr/Ca values are in the range of those reported for cocolithophores in other studies (Mejía et al., 2014 and refs, therein), and Mg/Ca, Al/Ca and Mg/Al show no evidence of diagenesis nor dolomitic calcite.

Site	Sr/Ca (mmol/mol)	Mg/Ca (mmol/mol)	Al/Ca (mmol/mol)	Mg/Al (mmol/mmol)
1093	2.22	11.82	26.89	0.44
1092	2.17	4.53	4.64	0.97
1122	2.21	24.20	23.04	1.05
1266	2.13	1.81	2.51	0.72
1226	2.28	4.86	15.22	0.32
U1338	2.07	3.17	21.77	0.15
U1337	1.98	5.99	40.76	0.15
1143	2.47	28.67	65.06	0.44
999	2.61	29.84	67.82	0.44
U1312	2.21	4.98	4.13	1.21
982	2.27	7.24	5.53	1.31
985	2.61	43.09	53.65	0.80
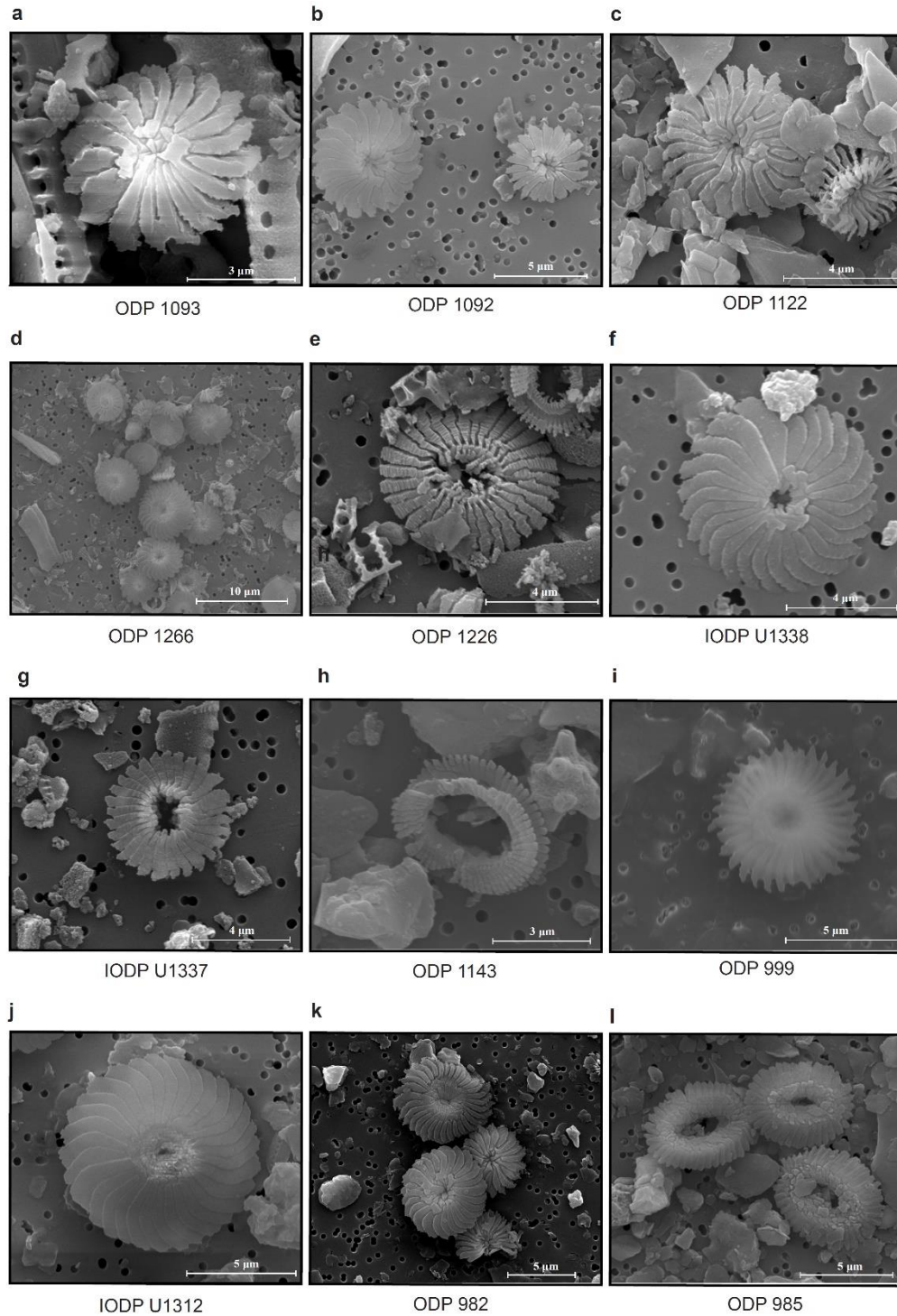
Supplementary Fig. A. Scanning Electron Microscope images of coccolith separations of sediment samples from ODP Site: **a)** 1093, **b)** 1092, **c)** 1122, **d)** 1266, **e)** 1226, **f)** IODP U1338, **g)** IODP U1337, **h)** ODP 1143, **i)** ODP 999, **j)** IODP U1312, **k)** ODP 982, and **l)** 985. Note that the < 8, < 10 and < 11 μm fractions contain the <2 μm fraction and therefore some small carbonate and clays are deposited on top of coccoliths. ODP 1143 was further separated and the measured fraction was 3-8 μm (image not shown).

Supplementary Note B. Selection of season of production in each Site

Tropical Equatorial Pacific upwelling region

The tropical Equatorial Pacific is one of the most complex oceanic systems, since ocean (e.g. Ekman divergence, shear instability, wave modes) and atmospheric processes (e.g. heat fluxes, wind stress and precipitation) influence each other, and consequently, also primary production (McClain et al., 2002). Upwelling in this region of the modern ocean (90-123.2 °W; 3.1 °S-3.8 °N) is seasonal, peaking during fall-winter (Honjo et al., 1995) (i.e. July-September), with satellite-derived chlorophyll *a* concentrations in the westernmost areas peaking the earliest, and in the easternmost areas peaking the latest (Dandonneau et al., 2004; McClain et al., 2002). The productivity maximum in the area is caused after the Inter-Tropical Convergence Zone (ITZC) migrates northward during boreal summer and upwelling intensifies (Dandonneau et al., 2004). Sediment traps from a nearby area at 5 °S and 140 °W (Broerse, 2000) also show the highest coccolith and coccosphere export during August-September, confirming that coccolithophore's productivity is likely coupled to nutrient input from upwelling processes in the region, most likely of Fe, and that highest primary productivities coincide with lowest water temperatures (McClain et al., 2002).

SeaWiFS satellite data from 1998 to 2001 show that the maximum chlorophyll *a* concentration for the nearby Sites IODP U1337 and U1338 occur during August (Dandonneau et al., 2004), which coincides with the satellite data of McClain et al. (2002). For this month and for both Sites, surface temperatures (0 m) obtained from the World Ocean Atlas (WOA, 2018) are the lowest (24.7-25.8 °C), but similar to those of July and September), while the mixed layer depth (potential density-derived, Monterey and Levitus, (1997) is the deepest (29-37 m). Being located more to the east and closer to the South-American coast, the peak of chlorophyll *a* seasonal cycle maximum arrives slightly later (McClain et al., 2002) for Site ODP 1226. Therefore, we selected August-September as the main production season at this Site. The influence of upwelling in temperature variability is larger compared to the more central Equatorial Sites IODP U1337 and U1338, which is evident in the larger temperature drop, reaching an August-September average of 20.9 °C during a period of deep mixed layer (30 m). Concomitant low SSTs and deep mixed layers indicate the strongest influence of upwelling processes, nutrient input, and productivity in the region (Supplementary Fig. B). From the Equatorial Pacific Sites here analyzed, ODP Site 1226 is the most affected by seasonality and therefore choosing the right season of production is especially important to compare to coccolith calcification Δ_{47}-derived temperatures.
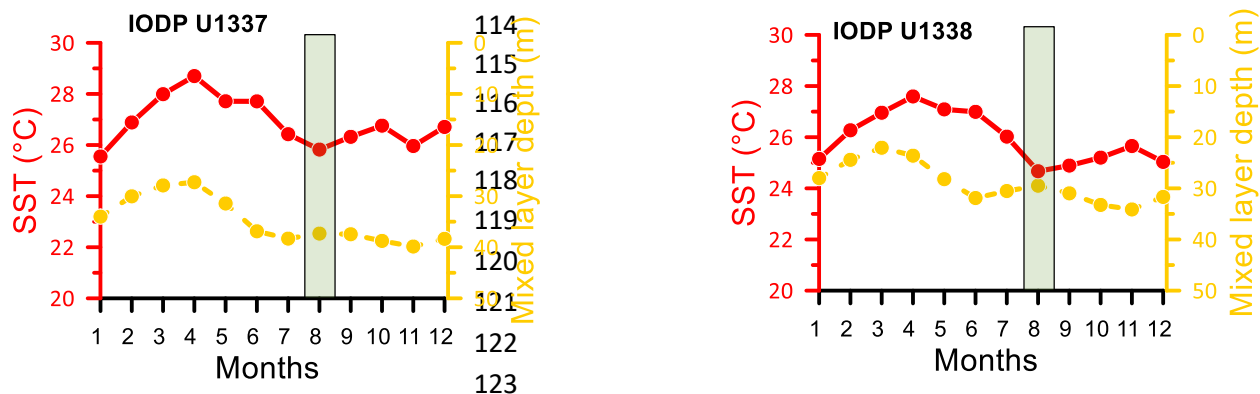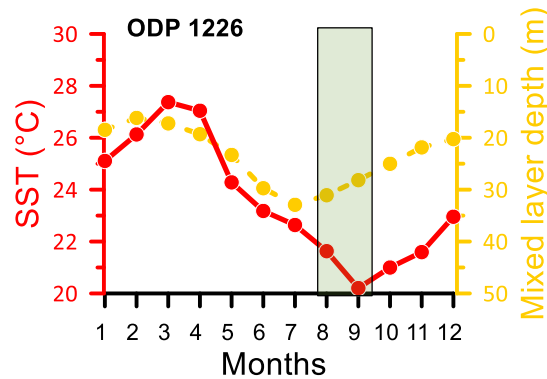
Supplementary Fig. B. World Ocean Atlas (WOA, 2018; 1955-2012) annual variability of SST (0 m) and mixed layer depth for Sites IODP U1337, U1338 and ODP Site 1226 in the tropical Equatorial Pacific. Green bar denotes months selected as main production season.

Tropical oligotrophic regions

Although relatively stable throughout the year in terms of temperature and productivity, the two tropical oligotrophic regions we consider in this study do show some seasonality. Chlorophyll *a* concentrations are low during the whole year in the Caribbean (Dandonneau et al., 2004). The main season of primary production in the Caribbean Colombian basin is controlled by the intensity of the South Caribbean Coastal Upwelling System (Andrade and Barton, 2005), which increases from January to March due to intensified trade winds in the Caribbean low level yet. Waters upwelled originate from the Subtropical Underwater, which is relatively low in nutrients (Correa-Ramirez et al., 2020). The influence of the foci located in the western upwelling zone of this system can reach northwestward locations, therefore also influencing seasonality in ODP Site 999. Similar to the tropical Equatorial Pacific Sites, the selected main season of production for ODP Site 999 (January-March) coincides with the lowest annual surface temperatures (average 26.6 °C) and deepest mixed layers (average 41 m) (Supplementary Fig. C), confirming the highest input of nutrients from upwelling processes.

As for the Caribbean, mean annual primary productivity in the South China Sea is also low (Liu and Chai, 2009). Physical-biogeochemical modelling (Liu and Chai, 2009) and sediment trap studies (Jin et al., 2019) show that coccolithophores and other primary producers peak during winter-early spring (December-March), in response to the nutrient input driven by the East Asian Winter Monsoon. The large air pressure difference between the Siberian High and the Aleutian Low enhances wind intensity and consequently, water mixing and nutrient input (Tseng et al., 2005). This process was shown to induce a six-fold increase of coccolithophore concentrations during the winter monsoon compared to the summer monsoon in the Northern South China Sea (Chen et al., 2007). In agreement with the most intense water mixing period, average temperatures during the selected main production season for ODP Site 1143 (December-March) were consistently the lowest (27.5 °C). The mixed layer depth in this location only varied from 25 to 35 m (Monterey and Levitus, 1997), with an average of 27 m for the chosen main production season (Supplementary Fig. C).

Due to the lower influence of upwelling processes in these tropical oligotrophic areas, the average temperature of the season chosen as the main production season (Site 999: 26.6 °C; Site 1143: 27.5 °C) do not differ very much from, for instance, mean annual temperatures (Site 999: 27.6 °C; Site 1143: 28.6 °C).

165 Therefore, they are not as critical when comparing to coccolith calcification Δ_{47}-derived temperatures as
166 compared to other Sites.
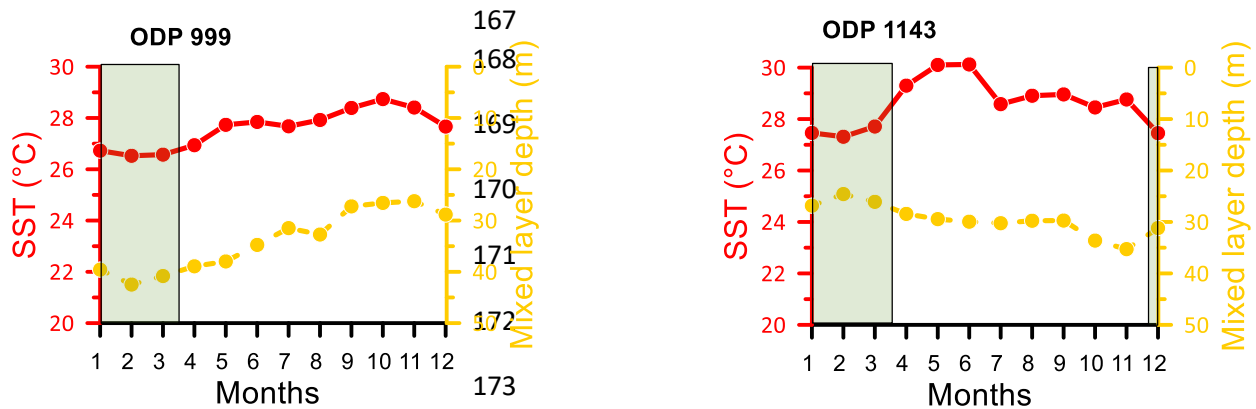
Supplementary Fig. C. World Ocean Atlas (WOA, 2018; 1955-2012) annual variability of variability of
SST (0 m) and mixed layer depth for Sites ODP Site 999 in the Colombian Caribbean, and ODP Site 1143
in Sothern South China Sea. Green bar denotes months selected as main production season.

North Atlantic mid and high latitudes

179   Since primary producers need both nutrients and light to thrive, and months with light availability are
180 limited in the most poleward-located areas, the main season of production at very high latitude sites
181 generally occur after spring and more towards summer. This general trend implies that peak production
182 occurs earlier as latitude decreases in both hemispheres (Dandonneau et al., 2004). Satellite, derived
183 oceanographic, and *in situ* data for the Azores region from 2003-2013, which is located nearby our mid-
184 latitude IODP Site U1312, show peaks of chlorophyll *a*, particulate inorganic and organic carbon and net
185 primary production during spring (April-May; Amorim et al. (2017)). Although for this area a second peak
186 in chlorophyll *a* can sometimes be identified during autumn (Dandonneau et al., 2004), here we focus on
187 the main spring bloom and select it as the main production season. This agrees with the highest
188 coccolithophore abundances and biomass during April observed close to one of the northernmost Azores
189 islands (Tercerira Island) (Narciso et al., 2016), which, as IODP Site U1312, is influenced by the North
190 Atlantic Current, which flows southwards from 45 to 40 °N and carries cold, nutrient-rich subpolar waters.
191 We therefore selected April-May as the main season of production for our North Atlantic mid-latitude Site
192 U1312, when surface temperatures are still low (14.5 °C) and similar to those of March, and the water
193 column is stabilizing from the strong mixing of winter months (average mixed layer depth 52 m)
194 (Supplementary Fig. D).
195   Following Dandonneau et al. (2004) hypothesis of light limitation for primary producers in high
196 latitudes, further north of IODP Site 1312, the main season of coccolithophore production at ODP Site 982
197 (at 57.5 °N) would be expected to be shifted towards summer. However, several studies using satellite and
198 float data, direct biomass observations, and sediment trap data, have shown that surface seasonal production
199 in the North Atlantic is still concentrated during the spring season at these latitudes (e.g. Behrenfeld et al.,
200 2013; Broerse, 2000; Mignot et al., 2018), although it may extend until June or even July (Behrenfeld et
201 al., 2013). Recent productivity studies in the North Atlantic have recently suggested that deep primary
202 production is significantly higher than usually acknowledged, and that it occurs during a longer season,

203   which extends from winter until spring (Behrenfeld et al., 2013). Considering a potential lag of 1-2 months
204   due to settling times of coccoliths (Newton et al., 1994), maximum coccolith export in the nearby sediment
205   trap NABE-48 (1 km depth) during March-May (Broerse, 2000) would be compatible with winter-spring
206   production. Therefore, for ODP Site 982, we selected the main season of production to extend form
207   December to June, with an earlier start and a later end compared to IODP Site U1312. Despite the
208   uncertainty in the exact duration of the main season of production for this site, average December-June
209   SST's (9.6 °C; (Supplementary Fig. D)) are indistinguishable from average March-June SST's (9.7 °C).
210   Selection of the precise extension of the main season of production for this location is therefore not critical
211   for comparison of Δ_{47}-derived temperatures.

212   Although light availability at ODP Site 982 (57.5 °N) is enough to trigger a spring-centered bloom,
213   primary producers at ODP Site 985 (69.9 °N) seem to be more light limited, and therefore the peak of
214   production is delayed to the summer season (Dandonneau et al., 2004). Total, carbonate and organic carbon
215   fluxes of a 1.9 km sediment trap in the nearby Greenland Basin (74 °N), located slightly north of ODP Site
216   985, are the highest during August-October (Honjo et al., 1987), suggesting peak production occurs at least
217   2-3 months earlier. We therefore chose July to be representative of the main season of production, when
218   surface temperatures are 6.9 °C and the mixed layer depth is at its shallowest (20 m) (Supplementary Fig.
219   D). Including August and September in the main production season, which are months with similar mixing
220   water conditions, does not change significantly average surface temperatures (7.3 °C).

221
222
223
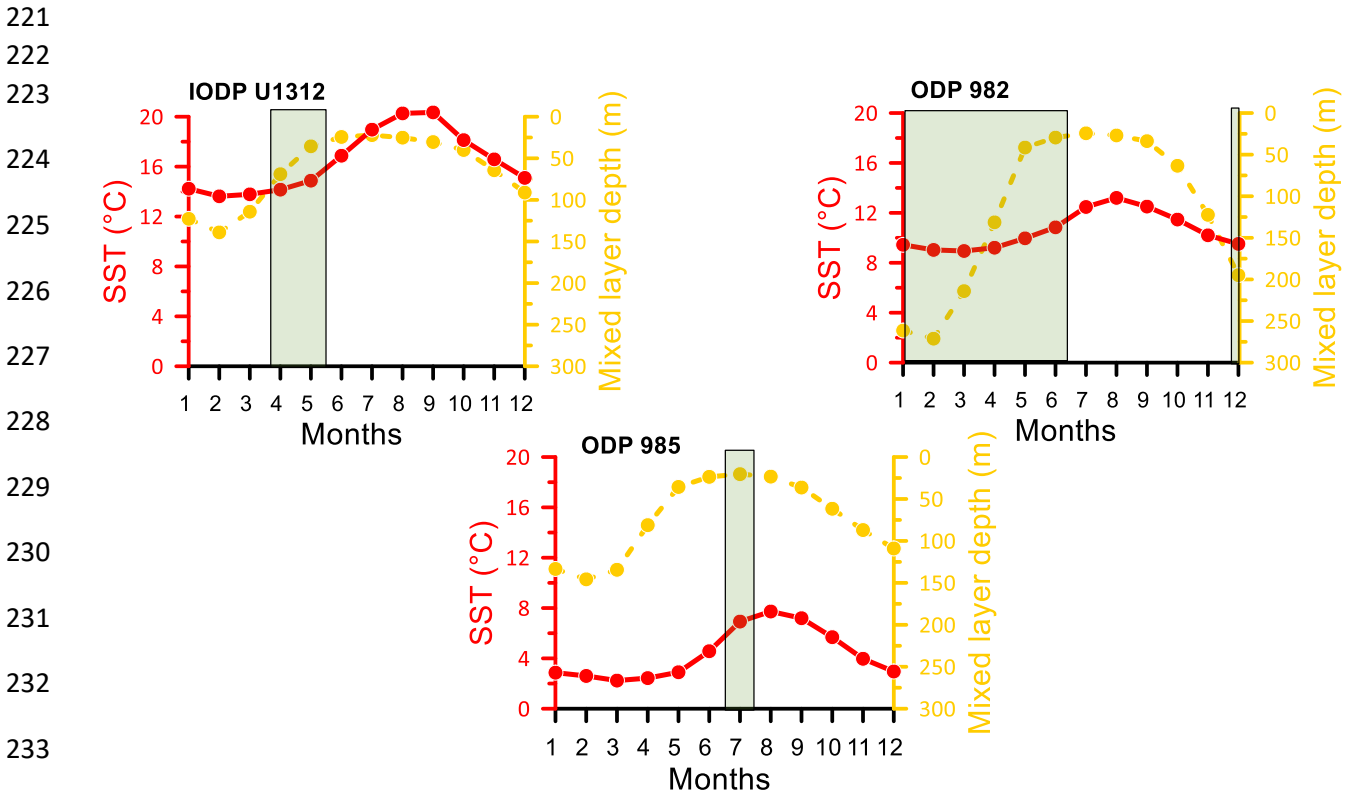
234   **Supplementary Fig. D.** World Ocean Atlas (WOA, 1955-2012) annual variability of variability of SST (0
235   m) and mixed layer depth for North Atlantic mid and high latitudes, for IODP Site U1312 northeast of the
236   Azores, ODP Site 982 at the Rockall Plateau, and ODP Site 985 at the Iceland Plateau. Green bar denotes
237   months selected as main production season.

238

240   Waters in the northwestern flank of the Walvis Ridge (ODP Site 1266) are generally considered
241 oligotrophic. Located in the eastern sector of the South Atlantic Gyre, waters in this Site are currently
242 mainly under the influence of the northwesterly-flowing oceanic branch of the Benguela Current, which
243 merges with the easterly-flowing South Atlantic Current at ~10 °E (Tangunan et al., 2020). This Site is
244 located, however, relatively close to the Benguela Upwelling System, which extends from 25-31 °S
245 (Shannon and Nelson, 1996). Satellite Chlorophyll *a* concentrations from the Benguela Upwelling System
246 show that seaward (westward) upwelling plumes peak during austral winters (August) (Romero et al.,
247 2002), while the additional productivity peak in summer remains close to the coast. Seaward winter
248 filaments could occasionally influence waters close to our Site, as they can extend up to 1000 km from the
249 upwelling foci (Shannon and Nelson, 1996). A winter season of production is supported by the highest
250 satellite-derived Chlorophyll *a* values during August-September for our ODP Site 1266 (Dandonneau et
251 al., 2004). Therefore, although productivity along the Benguela Coastal Current is much higher than that
252 along the Benguela Oceanic Current, exceptional winter productivity filaments likely influence seasonality
253 in ODP Site 1266. We chose August-September as the main season of primary production for this location,
254 which coincides with the lowest annual surface temperatures (average of 17.5 °C) and a period of a
255 stabilizing but still deep mixed layer (78 m) (Supplementary Fig. E).
256   Further south, our three remaining Sites are located in the western Pacific sector (ODP Site 1122) and
257 the Atlantic sector (ODP Sites 1092 and 1093) of the Southern Ocean. In the Southern Ocean, the main
258 season of production depends on the location of the Site within a series of fronts; the Subtropical, the
259 Subantarctic, the Polar and the Antarctic Circumpolar Current fronts (Orsi et al., 1995). This subdivides the
260 Southern Ocean into the Subantarctic zone (ODP Site 1122), the Polar Frontal zone (ODP Site 1092), and
261 the Antarctic zone (ODP Site 1093).
262   From these zones, the Subantarctic is the largest, most productive and most diverse in terms of
263 coccolithophores, and is the boundary between the warm oligotrophic subtropical gyres and the cold,
264 diatom-rich waters south of the polar front (Rigual-Hernández et al., 2020). Coccolith and coccosphere
265 fluxes in the SAM sediment trap located right at the location of ODP Site 1122 (at 1500 m), show maximum
266 values during austral summer (December-January). The summer timing of the main season of
267 coccolithophore production coincides with the highest satellite-derived PIC and chlorophyll *a*
268 concentrations (Rigual-Hernández et al., 2020), indicating fast coccolith settling times for this location and
269 therefore negligible delays compared to time of production. The average surface temperature during the
270 selected main season of production (December-January) is amongst the highest of the year (13.9 °C) during
271 a time of shallow mixed layer (34 m) (Supplementary Fig. E).
272   Particle export fluxes of the AESOPS sediment traps deployed in the Western Pacific sector of the
273 Southern Ocean (170 °W), show that south of the Subantarctic front, carbonate fluxes decrease, opal fluxes
274 increase, and although the onset of maximum particle export also occurs during austral summer, it is delayed
275 towards more southerly locations (Honjo et al., 2000). The AESOPS sediment trap MS-2 located in the
276 Polar Frontal zone, which is expected to show similar oceanographic conditions to those of ODP Site 1092,
277 also located in the same belt of the Southern Ocean, show peak inorganic carbon fluxes from November to
278 February (Honjo et al., 2000). On the other hand, being located in the Antarctic zone, south of the Polar
279 front, waters at ODP Site 1093 probably show intermediate characteristics compared to AESOPS sediment
280 traps MS-3 and MS-4. Therefore, a delayed main season of production compared to ODP Site 1092 from
281 December to March is expected from the observed peaks of inorganic carbon fluxes of sediment traps MS

3 and 4 (Honjo et al., 2000). The temperature and mixed layer profiles for ODP Sites 1092 and 1093 and
very similar, and in both cases, the selected main season of production shows the highest annual average
temperatures (1092: 6.3 °C; 1093: 4.1°C), during a period of relatively shallow average mixed layer (1092:
55 m; 1093: 69 m) (Supplementary Fig. E).
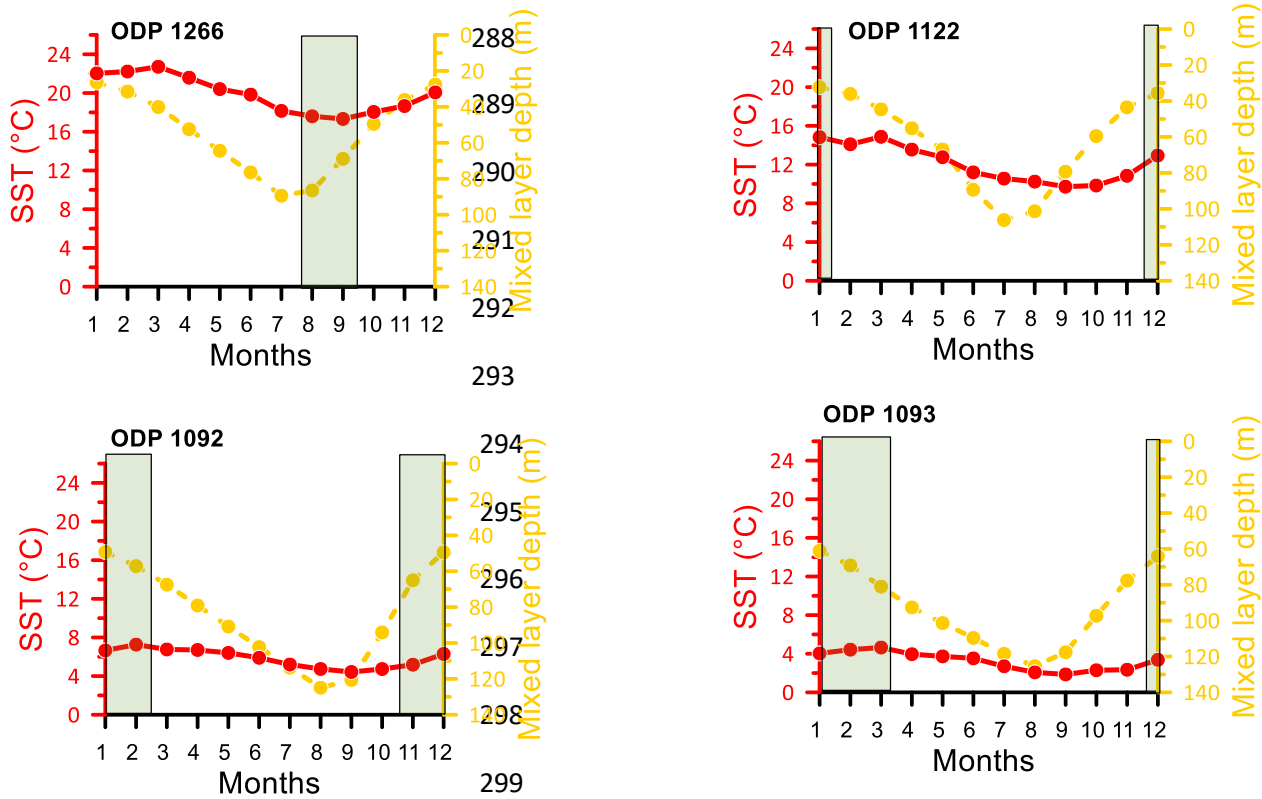
Supplementary Fig. E. World Ocean Atlas (WOA, 2018; 1955-2012) annual variability of variability of
SST (0 m) and mixed layer depth for South Atlantic and Southern Ocean locations, for ODP Site 1266 in
the Walvis Ridge, ODP Site 1122 in the western Pacific sector of the Southern Ocean (Subantarctic zone),
and ODP Sites 1092 (Polar Frontal zone) and 1093 (Antarctic zone) in the Atlantic sector of the Southern
Ocean. Green bar denotes months selected as main production season.
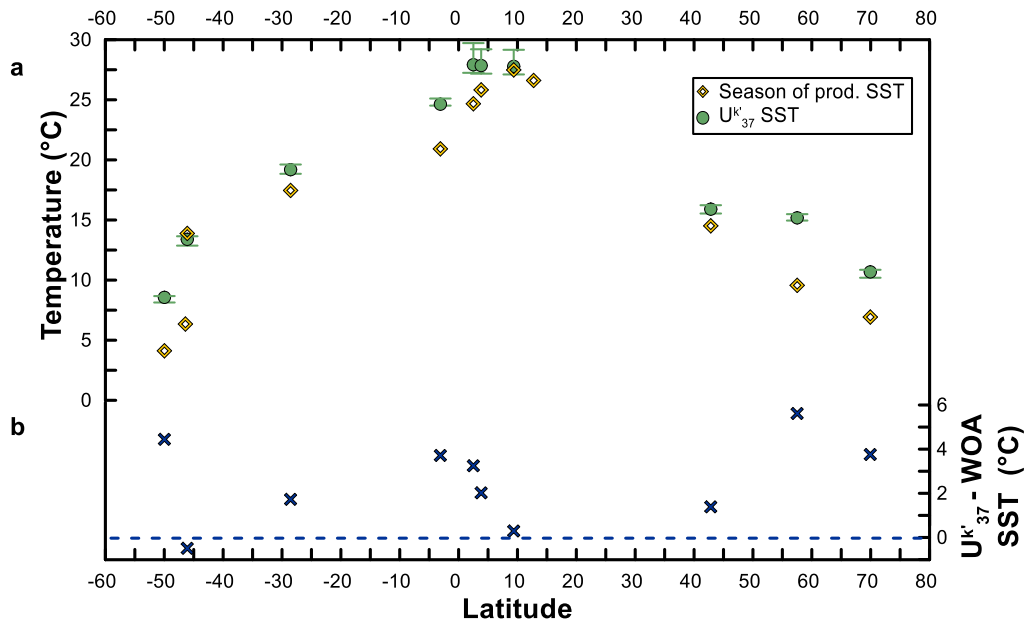
Supplementary Fig. F. a) Average WOA SSTs during the months of peak production (yellow diamonds) and estimated SSTs from $U^{k'}_{37}$ ratios (green circles) for each of our locations. $U^{k'}_{37}$-derived temperatures were estimated using the core top (Müller et al., 1998), bayspline (Tierney and Tingley, 2018), and the 55a *Emiliania huxleyi* batch culture (Prahl et al., 1988) calibrations, and error bars denote the maximum and the minimum SST values. **b)** Difference between WOA season of production SSTs and $U^{k'}_{37}$-derived SSTs (blue cross). This calculation considers $U^{k'}_{37}$-SSTs estimated using the calibration that leads to medium values compared to the other two calibrations. Blue dashed line show that most of the $U^{k'}_{37}$-derived SSTs are warmer than the actual SSTs during the season of production.

Supplementary Note C. Application of abiogenic and culture coccolith Δ₄₇ calibrations to estimate calcification temperatures

When we apply the most recent abiogenic calibration (Anderson et al., 2021) to our coccolith Δ_{47} we generally obtain the coldest calcification temperatures (Table 1b, main text), except for IODP Site U1337, where temperatures were 0.2 °C higher than those derived from Meinicke et al. (2021) (these calibration curves cross each other at the highest temperature end; Fig. 5b). Therefore, the average difference between $U^{k'}_{37}$ and Δ_{47}-derived temperatures is also the highest (6.8 °C, Supplementary Fig. G).

Colder calcification temperatures derived from the abiogenic calibration (Anderson et al., 2021) would imply even deeper habitats than those inferred from the application of the foraminifera calibration (Supplementary Fig. H). These temperatures still suggest that coccolithophores' production lies within the euphotic zone in upwelling tropical Sites, but below it in oligotrophic tropical Sites. The much colder average calcification temperatures at high latitude Sites obtained with the abiogenic calibration (Anderson

330 et al., 2021) imply unrealistic habitat depths well below the euphotic zone, where coccolithophores cannot

331 photosynthesize (Supplementary Fig. H).

332   Applying the culture coccolith Δ_{47} calibration (Katz et al., 2017) to our dataset assumes comparability

333 between gas standardized and carbonate standardized (this study) Δ_{47} data. While there is some uncertainty

334 due to the lack of carbonate standardization at the IPGP laboratory, where data from the culture calibration

335 come from, the values of ETH-1 reported in Bonifacie et al. (2017) (0.197‰.) is within error of the I-CDES

336 value of Bernasconi et al. (2021) (0.205 ‰), and the reported value of sample 102-GC-AZ01b (0.625 ‰

337 CDES90) in Katz et al. (2017) is very close to the value of 0.620 ‰ (I-CDES) reported by Upadhyay et al.

338 (2021). In addition, the data of the Katz et al. (2017) calibration fall well within the sample population of

339 the Meinicke et al. (2021) calibration, supporting the high quality of those data and the lack of vital effects

340 in coccolithophores.

341   Application of the culture calibration leads to the warmest calcifying temperatures. Although at first,

342 calcification temperatures derived from this calibration would imply a more surface habitat for most Sites,

343 as opposed to the deeper coccolithophore habitat inferred from the foraminifera calibration discussed in the

344 main text (Meinicke et al., 2021), average values obtained using the Katz et al. (2017) calibration even

345 overestimate SSTs during the season of production in 8 of our Sites (Supplementary Fig. G and H).

346 Applying this warmest Δ_{47} calibration to coccolith Δ_{47} data from ODP Sites 1122 and 1266 lead to average

347 calcifying temperatures which, as by using the Meinicke et al. (2021) calibration, still locate

348 coccolithophores at depths below the euphotic zone, where no photosynthesis can occur. Since in most of

349 our locations $U^{k'}_{37}$-derived temperatures also overestimate SSTs, using this Δ_{47} calibration reduces the

350 average difference between $U^{k'}_{37}$ and Δ_{47} estimations to 2° C (Supplementary Fig. G). From the Δ_{47}

351 calibrations available, the Katz et al. (2017) is the less well constrained due to the relatively low sample

352 (and standard) replication as well as the limited range of temperatures of the cultures. For this reason, it is

353 difficult to use derived temperatures to pinpoint a specific habitat depth. Therefore, given that using this

354 calibrationClick or tap here to enter text. leads to average calcification temperatures that are either too hot

355 (for 8 Sites) or still too cold (for 2 Sites), we do not consider it further. In fact, Katz et al. (2017) already

356 suggested that a calibration with more datapoints should be used.

357   The extremely low calcification temperatures derived from the abiogenic Δ_{47} calibration (Anderson et

358 al., 2021) for high latitude Sites could potentially suggest that at least at the cold end of coccolithophores'

359 surviving temperatures, there may be some biological overprints in coccolith Δ_{47}. This, and the generally

360 unrealistic warm average calcification temperatures derived from the available coccolith culture calibration

361 (Katz et al., 2017), highlights the potential necessity of conducting a better statistically-constrained culture

362 calibration, in which sample replication is much higher, carbonate standards are used, and growth ocean

363 conditions (i.e. light settings) are better mimicked. Significant improvements in analytical precision

364   suggests that the potential for some vital effects may need to be re-evaluated with more precise analysis of
365   culture, sediment trap, or ocean samples. Whether the potential overprint in coccolith Δ_{47} is consistent with
366   that produced by biomineralization from foraminifera at the cold temperature range, is something that
367   remains to be investigated.

368
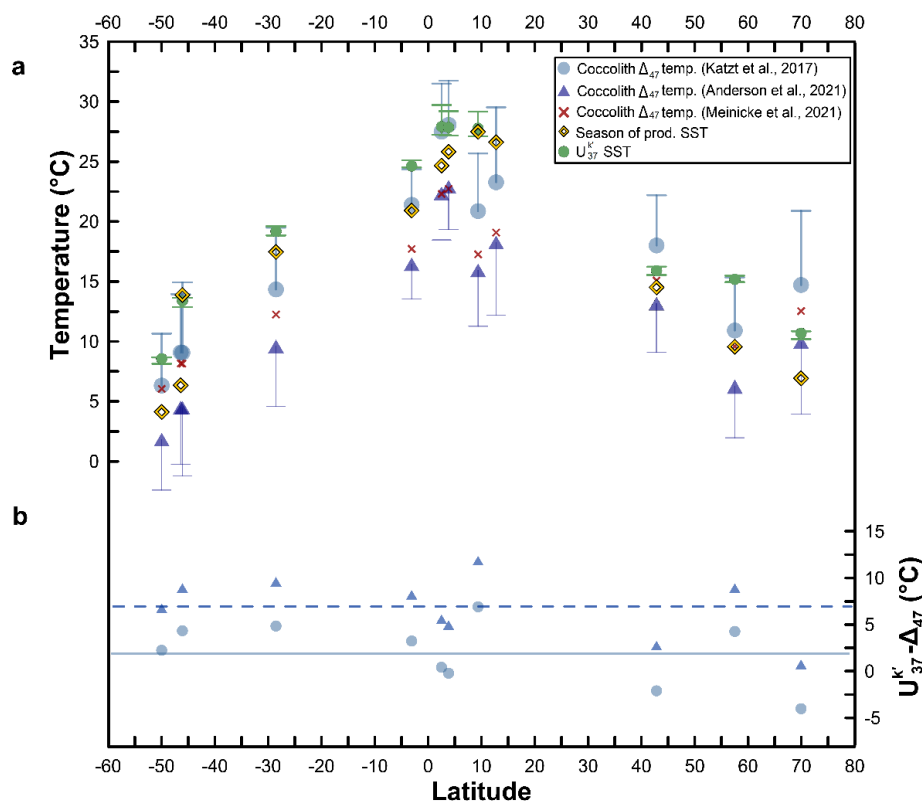
369   **Supplementary Fig. G. a)** Estimated calcification temperatures from coccolith Δ_{47} using the Δ_{47}
370   calibrations of Katz et al. (2017); light blue circles, of Anderson et al. (2021); dark blue tringles, and of
371   Meinicke et al. (2021): red cross, SSTs from $\mathbf{U_{37}^{k'}}$ (green circles), and average WOA SSTs during the months
372   of peak production (yellow diamonds) for each location. $\mathbf{U_{37}^{k'}}$-derived SSTs were estimated with the Müller
373   et al. (1998), the Tierney and Tingley (2018), and the Prahl et al. (1988) calibrations, and error bars denote
374   the maximum and the minimum SST values. Error bars of Δ_{47} calcification temperatures are to the 95%
375   (CI). To improve readability, only positive errors, and only negative errors are shown for temperatures
376   estimated using the coccolith culture and the abiogenic culture calibrations, respectively. No error bars are
377   shown for calcification temperatures derived from the foraminifera calibration (see details in Fig. 3). **b)**
378   Difference between $\mathbf{U_{37}^{k'}}$-derived SSTs and coccolith Δ_{47}-derived calcification temperatures using the
379   coccolith culture (light blue circles) and the abiogenic (dark blue tringles) calibrations. This calculation
380   considers $\mathbf{U_{37}^{k'}}$-SSTs estimated using the calibration that leads to medium values compared to the other two
381   calibrations. Solid dark blue and dashed light blue lines show that on average $\mathbf{U_{37}^{k'}}$-SSTs are 6.8 and 2 °C
382   warmer than coccolith Δ_{47} calcification temperatures derived from the abiogenic and the coccolith culture
383   Δ_{47} calibrations, respectively.

384

385
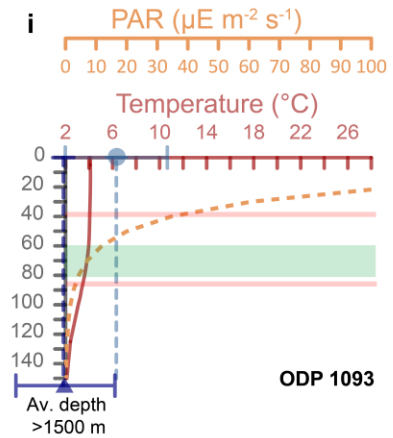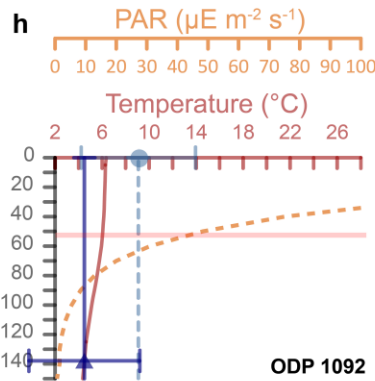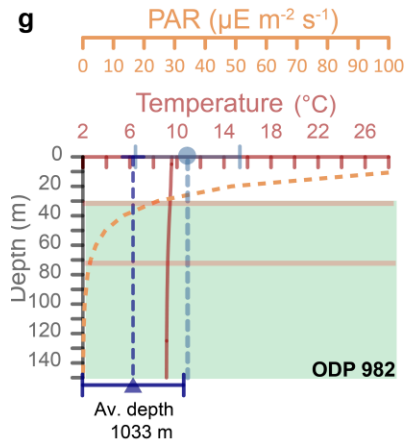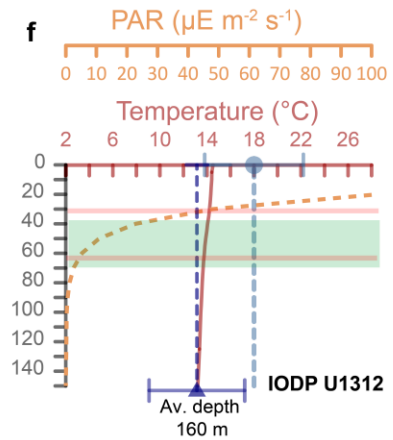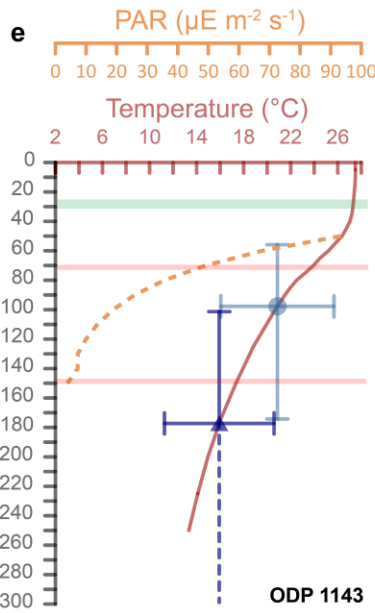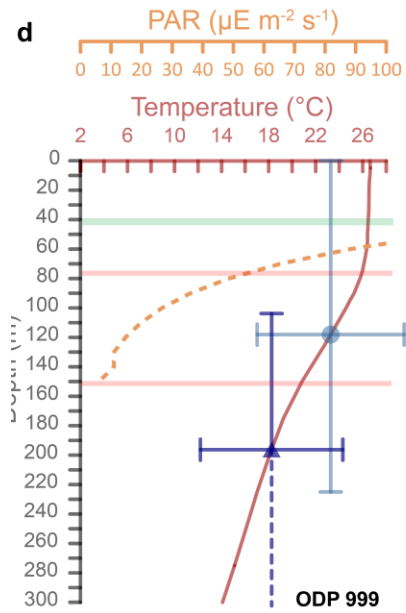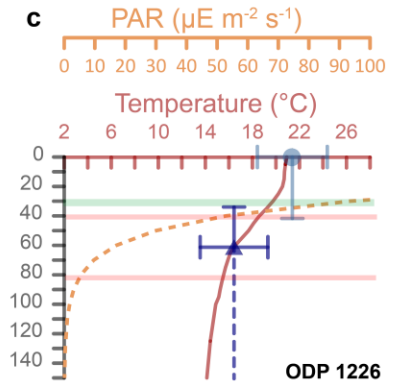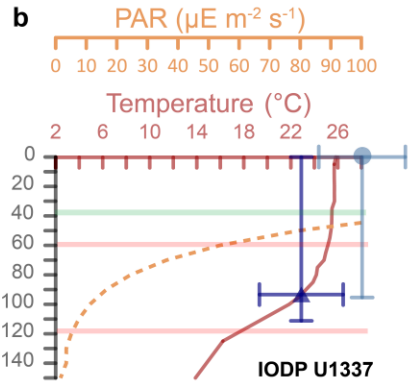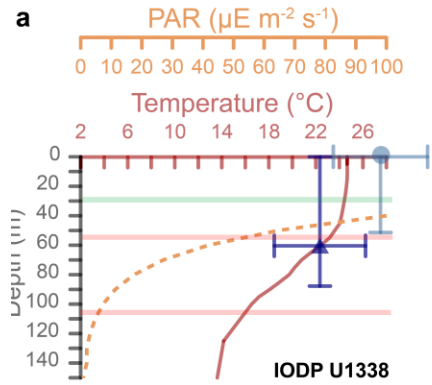
386 **Supplementary Fig. H.** Vertical profile of ocean temperature (solid red line) and photosynthetic active
387 radiation (PAR; dashed orange line, $\mu E\,m^{-2}\,s^{-1}$) at our different locations. Coccolith Δ_{47}-derived calcification
388 temperatures obtained applying the abiogenic (Anderson et al., 2021; dark blue triangles) and the coccolith
389 culture (Katz et al., 2017; light blue circles) locate the likely habitat depth of coccolithophores in each Site.
390 Horizontal error bars indicate the possible range of calcification temperature variation (95% CI). We use
391 these warmest and coldest calcification temperatures to determine the potential shallowest and deepest
392 habitats, respectively, here denoted by vertical error bars. Dashed vertical error bars indicate a potential
393 habitat depth outside the depth scale in the y axis. Green shaded area indicates the seasonal variation of the
394 base of the mixed layer during the selected months of peak production. Horizontal red lines comprise the
395 depth where PAR varies between 10% and the limit of the euphotic zone (1%), below which
396 coccolithophores are likely not living.

397

398 **Supplementary Note D. Presence of sub-euphotic zone species and non-coccolith carbonate**

399   Ideally, calcification temperatures obtained from Δ_{47} should isolate the signal from species uniquely

400 relying on photosynthesis and therefore inhabiting the euphotic zone. However, obtaining pure euphotic

401 zone coccolith separations from sediments can be difficult. Some coccolithophore species can inhabit

402 depths well below the euphotic zone (subeuphotic zone species <1% PAR), where nutrients are plenty but

403 light is limiting (Poulton et al., 2017). At these low light settings, their peak abundance suggests that these

404 species may rely in mixotrophy or phagotrophy for survival (Brand, 1994).

405   Average Δ_{47} calcification temperatures for the two tropical oligotrophic Sites (ODP Site 999 and 1143)

406 suggest habitats slightly below the euphotic zone (2-29 m below 1% PAR), where photosynthetic organisms

407 cannot survive. Therefore, here we evaluated quantitatively the sediment contents that could have

408 introduced a slight cold bias in our measurements, which if corrected, could locate coccolithophores' habitat

409 within the euphotic zone. For this, we quantified the relative abundance and carbonate contribution of

410 coccolithophore species living above the lower limit of the euphotic zone, including the upper euphotic

411 zone ones, altogether here denoted as LEZ, subeuphotic zone species (SEZ) and no-coccolith carbonate

412 (NN) for the two tropical oligotrophic Sites (Supplementary Fig. I). A quicker qualitative analysis using

413 light microscope of other Sites suggested that cold biases introduced by the presence of some subeuphotic

414 zone species or non-coccolith carbonate could not explain the extremely large differences between SSTs

415 and Δ_{47} calcification temperatures in Sites 1122 and 1266 (5.2 and 5.7 °C, respectively), locations where

416 the thermocline is rather small and therefore inferred habitats for photosynthetic organisms are unrealistic.

417 Moreover, although there is presence of some non-coccolith carbonate, presumably from foraminifera, at

418 the upwelling Sites IODP U1337 and U1138, these were also qualitatively not found to be abundant enough

419 to drive inferred habitat depths up the surface.

420   Quantitatively relevant $CaCO_3$ contributions from the subeuphotic zone species *Florisphaera profunda*

421 are present in the ODP Site 999 coccolith separation (~17%, (Supplementary Fig. I)). This species typically

422 inhabits depths of ~200 m (Beaufort et al., 2008), where temperatures at this site can be up to up to ~12 °C

423 colder than at the surface during some months of the year (8.5 °C colder during the chosen season of

424 production). Despite this large surface-deep temperature difference, a nearly pure *F. profunda* assemblage

425 would be required to explain the 7.5 °C difference between our Δ_{47} calcification temperatures and season

426 of production SSTs. Therefore, the presence of subeuphotic zone species cannot explain the whole

427 magnitude of difference between SST and Δ_{47} calcification temperatures, and hence, we can rule out a

428 surface habitat of photosynthesizing coccolithophores for this Site. Further locations with presence of *F.*

429 *profunda* include ODP Sites 1143, 1226 and 1266, but $CaCO_3$ contribution from this species are clearly

430 lower than at ODP Site 999. *Ceratholitus cristatus* has been found to inhabit depths between 100-200 m in

431 the Mediterranean (Knappertsbusch, 1993), and is suggested to belong to the deep dwelling taxa also in

432 Equatorial Pacific waters (Broerse, 2000). Therefore, this species could potentially contribute to a cold bias

433 in Sites U1337, U1338, 999, 1143 and 1266. Here we group this species together with the rest of the lower

434 photic zone taxa mostly growing between 1-10% PAR, following Poulton et al. (2017) (hence, as LEZ).

435 Despite the large thickness and size of *C. cristatus* placoliths, their rare abundance in all assemblages entails

436 only limited $CaCO_3$ contribution to the total carbonate (up to 3% at Site 999). Therefore, the potential cold

437 bias from their placoliths is likely insignificant.

438 The presence of non-coccolith calcite in our separations, if produced by organisms inhabiting deeper

439 waters than coccoliths, could also bias the inferred coccolith Δ_{47} calcification temperatures towards colder

440 than actual values. In separations of ODP Sites 999 and 1143 we identified fragments of calcareous

441 dinoflagellates, which have been reported abundant in the Equatorial and tropical Atlantic at depths between

442 50-100 m (Karwath et al., 2000). Since these depths are not deeper than the habitat inferred from coccolith

443 Δ_{47} calcification temperatures for these Sites, and since they showed only a small $CaCO_3$ contribution to

444 the total assemblage (<1%), no significant cold bias is expected from their presence. Further unidentifiable

445 carbonate fragments, which were by far most abundant at upwelling IODP Sites U1337 and U1338, could

446 either belong to coccoliths, or to planktonic foraminifera. The rather modest difference between the inferred

447 Δ_{47} calcification temperatures and SSTs at these locations (2.4-3.1 °C) compared to the oligotrophic Sites

448 is consistent with only small contributions from benthic foraminifera fragments. We do not expect

449 significant cold biases due to planktonic foraminifera fragments, as these are likely living at similar depths

450 as those inferred for coccolithophores from Δ_{47} calcification temperatures.

451

452

453

454
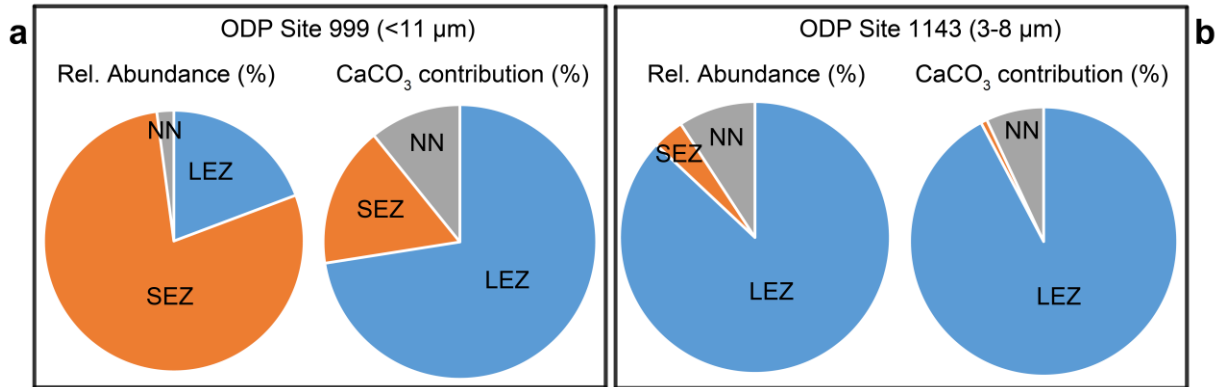
Supplementary Fig. I. Relative abundances (%) and CaCO$_3$ contributions (%) of coccolithophore species living within the euphotic zone (LEZ), subeuphotic zone coccolith species (SEZ), and non-coccolith carbonate (NN) in tropical oligotrophic ODP Sites **a)** 999, **b)** 1143.

458

459
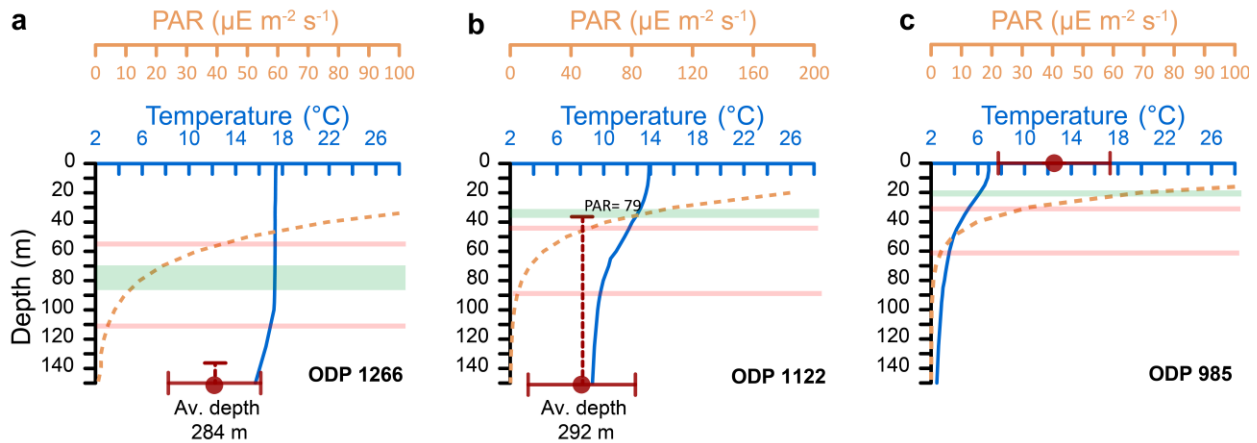
Supplementary Fig. J. Vertical profile of ocean temperature (solid blue line) and photosynthetic active radiation (PAR; dashed orange line, μE m^{-2} s^{-1}) at Sites **a)** ODP 1266, **b)** 1122, and **c)** 985. Coccolith Δ_{47}-derived calcification temperatures obtained applying the foraminifera calibration (Meinicke et al., 2021) (red) locates the likely habitat depth of coccolithophores in each Site. Horizontal error bars indicate the possible range of calcification temperature variation (95% CI). We use these warmest and coldest calcification temperatures to determine the potential shallowest and deepest habitat, respectively, here denoted by vertical error bars. Dashed vertical error bars indicate a potential habitat depth outside the depth scale in the y axis. Green shaded area indicates the seasonal variation of the base of the mixed layer during the selected months of peak production. Horizontal red lines comprise the depth where PAR varies between 10% and the limit of the euphotic zone (1%), below which coccolithophores are likely not living. Unrealistic habitat depths (average value noted in figure) are indicated by cold coccolith Δ_{47}-derived calcification temperatures for ODP Sites 1266 and 1122, while warmer calcification temperatures than SSTs were found for ODP Site 985.

473

474

Supplementary Table E. p-values for testing differences between regression slopes and intercepts, including the coccolith core top Δ_{47} regression (this study), the mixed foraminifera calibration (Meinicke et al., 2021), and the latest abiogenic calibration (Anderson et al., 2021). Values > 0.05 indicate that slopes and/or intercepts of two given regressions are not significantly different (null hypothesis: slope or intercept equation A = slope or intercept equation B).* Only with <40 °C dataset. When the whole dataset is included, these calibrations show no differences (Peral et al., 2022).

Regression A	Regression B	p_{slope}	$p_{interncept}$
Coretop coccolith (this study)	Coretop Foram. (Meinicke et al., 2021)	**<0.05**	**<0.05**
Coretop coccolith (this study)	Abiogenic <40 °C (Anderson et al., 2021)	0.11*	0.08*
Coretop Foram. (Meinicke et al., 2021)	Abiogenic <40 °C (Anderson et al., 2021)	**<0.05***	**<0.05***

481

Supplementary Note E. Snapshot into alternative Alkenone calibrations: are alkenones also produced at depth?

Our coccolith Δ_{47} dataset implies calcification takes place at depth in tropical regions, or within the mixed layer in higher latitudes. We explored the possibility of alkenones being also produced under the same temporal and depth ranges. For this, we used a totally independent $U^{k\prime}_{37}$ dataset from a subset of Sites used by the most recent alkenone calibration work of Tierney and Tingley (2018), which overlap geographically with the Sites in this study. We then calculated alternative $U^{k\prime}_{37}$ calibrations to those published, which use mean annual SST (Tierney and Tingley, 2018; Müller et al., 1998), by using: a) SSTs during the season of production, and b) temperatures of calcification at depth during the season of production, as inferred from our coccolith Δ_{47} dataset. For the second case, we used the inferred coccolithophores' habitat depth from coccolith Δ_{47} of our tropical Sites to determine the average season of production temperatures at those depths for the tropical geographical locations of Tierney and Tingley (2018) coinciding with our Sites. In the case of high latitude Sites, we calculated the average season of production temperatures of the mixed layer depth. The regressions are shown in Supplementary Fig. K.

When we apply these new independent calibrations, which consider seasonal and subsurface production, to our $U^{k\prime}_{37}$ values, as expected, we observe that our $U^{k\prime}_{37}$-derived temperatures are in a closer agreement to coccolith Δ_{47} calcification temperatures calculated using the foraminifera Δ_{47} calibration. When seasonal production is considered, the difference between $U^{k\prime}_{37}$-derived SSTs and coccolith Δ_{47} calcification temperatures decreases from 4.7 to 3.0 °C. This difference decreases even more when seasonal temperatures at inferred depths are considered (-0.9 °C). This shows how it might be possible to establish future alkenone calibrations contemplating subsurface depth and seasonal production.

503

504
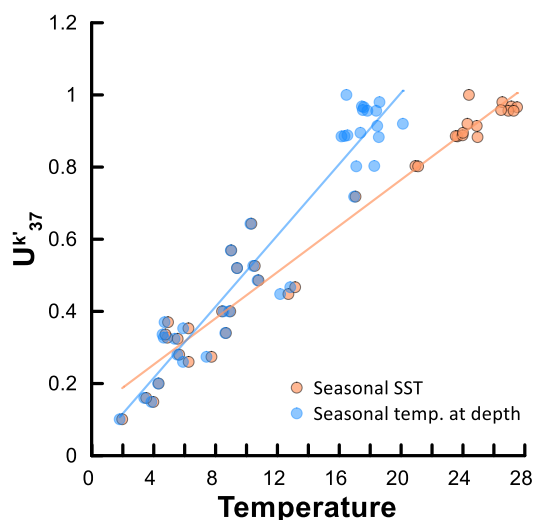
505
506

507   **Supplementary Fig. K. $U_{37}^{k\prime}$** as a function of **a)** sea surface temperatures (SST) during the season of
508   production ($U_{37}^{k\prime} = 0.032 * T + 0.1246$; R = 0.9749; p < 0.0001), and **b)** calcification temperature, as inferred
509   from our coretop coccolith Δ_{47} dataset, during the season of production ($U_{37}^{k\prime} = 0.0494 * T + 0.0181$; R =
510   0.9579; p < 0.0001). Data include only Sites in the Tierney and Tingley (2018) dataset which coincide
511   geographically with the Sites described in this study, from which we have studied oceanographic conditions
512   and seasonality.

513

514   **Supplementary References**

515

516   Amorim, P., Perán, A.D., Pham, C.K., Juliano, M., Cardigos, F., Tempera, F., Morato, T., 2017. Overview
517   of the ocean climatology and its variability in the Azores region of the North Atlantic including
518   environmental characteristics at the seabed. Front Mar Sci 4, 56.
519   https://doi.org/10.3389/FMARS.2017.00056/BIBTEX

520   Anderson, N.T., Kelson, J.R., Kele, S., Daëron, M., Bonifacie, M., Horita, J., Mackey, T.J., John, C.M.,
521   Kluge, T., Petschnig, P., Jost, A.B., Huntington, K.W., Bernasconi, S.M., Bergmann, K.D., 2021. A
522   Unified Clumped Isotope Thermometer Calibration (0.5–1,100°C) Using Carbonate-Based
523   Standardization. Geophys Res Lett 48, e2020GL092069. https://doi.org/10.1029/2020GL092069

524   Andrade, C.A., Barton, E.D., 2005. The Guajira upwelling system. Cont Shelf Res 25, 1003–1022.
525   https://doi.org/10.1016/J.CSR.2004.12.012

526   Beaufort, L., Couapel, M., Buchet, N., Claustre, H., Goyet, C., 2008. Calcite production by
527   coccolithophores in the south east Pacific Ocean. Biogeosciences 5, 1101–1117.
528   https://doi.org/10.5194/bg-5-1101-2008

529   Behrenfeld, M.J., Doney, S.C., Lima, I., Boss, E.S., Siegel, D.A., 2013. Annual cycles of ecological
530   disturbance and recovery underlying the subarctic Atlantic spring plankton bloom. Global
531   Biogeochem Cycles 27, 526–540. https://doi.org/10.1002/gbc.20050

Bernasconi, S.M., Daëron, M., Bergmann, K.D., Bonifacie, M., Meckler, A.N., Affek, H.P., Anderson, N., Bajnai, D., Barkan, E., Beverly, E., Blamart, D., Burgener, L., Calmels, D., Chaduteau, C., Clog, M., Davidheiser-Kroll, B., Davies, A., Dux, F., Eiler, J., Elliott, B., Fetrow, A.C., Fiebig, J., Goldberg, S., Hermoso, M., Huntington, K.W., Hyland, E., Ingalls, M., Jaggi, M., John, C.M., Jost, A.B., Katz, S., Kelson, J., Kluge, T., Kocken, I.J., Laskar, A., Leutert, T.J., Liang, D., Lucarelli, J., Mackey, T.J., Mangenot, X., Meinicke, N., Modestou, S.E., Müller, I.A., Murray, S., Neary, A., Packard, N., Passey, B.H., Pelletier, E., Petersen, S., Piasecki, A., Schauer, A., Snell, K.E., Swart, P.K., Tripati, A., Upadhyay, D., Vennemann, T., Winkelstern, I., Yarian, D., Yoshida, N., Zhang, N., Ziegler, M., 2021. InterCarb: A Community Effort to Improve Interlaboratory Standardization of the Carbonate Clumped Isotope Thermometer Using Carbonate Standards. Geochemistry, Geophysics, Geosystems 22, e2020GC009588. https://doi.org/10.1029/2020GC009588

Bonifacie, M., Calmels, D., Eiler, J.M., Horita, J., Chaduteau, C., Vasconcelos, C., Agrinier, P., Katz, A., Passey, B.H., Ferry, J.M., Bourrand, J.J., 2017. Calibration of the dolomite clumped isotope thermometer from 25 to 350 °C, and implications for a universal calibration for all (Ca, Mg, Fe)CO3 carbonates. Geochim Cosmochim Acta 200, 255–279. https://doi.org/10.1016/j.gca.2016.11.028

Brand, L.E., 1994. Physiological ecology of marine coccolithophores, in: Winter, A.,, Siesser, W.G. (Eds.), Coccolithophores. Cambridge University Press, Cambridge, pp. 39–49.

Broerse, A.T.C., 2000. Coccolithophore export production in selected ocean environments: seasonality, biography, carbonate production. Vrije Unversiteit Amsterdam (VU)., Amsterdam.

Chen, Y. ling L., Chen, H.Y., Chung, C.W., 2007. Seasonal variability of coccolithophore abundance and assemblage in the northern South China Sea. Deep Sea Research Part II: Topical Studies in Oceanography 54, 1617–1633. https://doi.org/10.1016/J.DSR2.2007.05.005

Correa-Ramirez, M., Rodriguez-Santana, Á., Ricaurte-Villota, C., Paramo, J., 2020. The Southern Caribbean upwelling system off Colombia: Water masses and mixing processes. Deep Sea Research Part I: Oceanographic Research Papers 155, 103145. https://doi.org/10.1016/J.DSR.2019.103145

Dandonneau, Y., Deschamps, P.Y., Nicolas, J.M., Loisel, H., Blanchot, J., Montel, Y., Thieuleux, F., Bécu, G., 2004. Seasonal and interannual variability of ocean color and composition of phytoplankton communities in the North Atlantic, equatorial Pacific and South Pacific. Deep Sea Research Part II: Topical Studies in Oceanography 51, 303–318. https://doi.org/10.1016/J.DSR2.2003.07.018

Eiler, J.M., 2007. "Clumped-isotope" geochemistry-The study of naturally-occurring, multiply-substituted isotopologues. Earth Planet Sci Lett 262, 309–327. https://doi.org/10.1016/j.epsl.2007.08.020

Honjo, S., Dymond, J., Collier, R., Manganini, S.J., 1995. Export production of particles to the interior of the equatorial Pacific Ocean during the 1992 EqPac experiment. Deep Sea Research Part II: Topical Studies in Oceanography 42, 831–870. https://doi.org/10.1016/0967-0645(95)00034-N

Honjo, S., Francois, R., Manganini, S., Dymond, J., Collier, R., 2000. Particle fluxes to the interior of the Southern Ocean in the Western Pacific sector along 170°W. Deep Sea Research Part II: Topical Studies in Oceanography 47, 3521–3548. https://doi.org/10.1016/S0967-0645(00)00077-1

569 Honjo, S., Manganini, S.J., Karowe, A., Woodward, B.L., 1987. Nordic Seas Sedimentation Data File.
570   Volume 1. Particle Fluxes, North-Eastern Nordic Seas: 1983-1986., Defense Technical Information
571   Center.

572 Jin, X.B., Liu, C.L., Zhao, Y.L., Zhang, Y.W., Wen, K., Lin, S., Li, J.R., Liu, Z.F., 2019. Two Production
573   Stages of Coccolithophores in Winter as Revealed by Sediment Traps in the Northern South China
574   Sea. J Geophys Res Biogeosci 124, 2335–2350. https://doi.org/10.1029/2019JG005070

575 Karwath, B., Janofske, D., Willems, H., 2000. Spatial distribution of the calcareous dinoflagellate
576   Thoracosphaera heimii in the upper water column of the tropical and equatorial Atlantic. International
577   Journal of Earth Sciences 2000 88:4 88, 668–679. https://doi.org/10.1007/S005310050296

578 Katz, A., Bonifacie, M., Hermoso, M., Cartigny, P., Calmels, D., 2017. Laboratory-grown coccoliths
579   exhibit no vital effect in clumped isotope ($\Delta 47$) composition on a range of geologically relevant
580   temperatures. Geochim Cosmochim Acta 208, 335–353. https://doi.org/10.1016/j.gca.2017.02.025

581 Knappertsbusch, M., 1993. Geographic distribution of living and Holocene coccolithophores in the
582   Mediterranean Sea. Mar Micropaleontol 21, 219–247. https://doi.org/10.1016/0377-8398(93)90016-
583   Q

584 Liu, G., Chai, F., 2009. Seasonal and interannual variability of primary and export production in the South
585   China Sea: a three-dimensional physical–biogeochemical model study. ICES Journal of Marine
586   Science 66, 420–431. https://doi.org/10.1093/ICESJMS/FSN219

587 McClain, C.R., Christian, J.R., Signorini, S.R., Lewis, M.R., Asanuma, I., Turk, D., Dupouy-Douchement,
588   C., 2002. Satellite ocean-color observations of the tropical Pacific Ocean. Deep Sea Research Part II:
589   Topical Studies in Oceanography 49, 2533–2560. https://doi.org/10.1016/S0967-0645(02)00047-4

590 Meinicke, N., Reimi, M.A., Ravelo, A.C., Meckler, A.N., 2021. Coupled Mg/Ca and Clumped Isotope
591   Measurements Indicate Lack of Substantial Mixed Layer Cooling in the Western Pacific Warm Pool
592   During the Last ~5 Million Years. Paleoceanogr Paleoclimatol 36, e2020PA004115.
593   https://doi.org/10.1029/2020PA004115

594 Mejía, L.M., Ziveri, P., Cagnetti, M., Bolton, C., Zahn, R., Marino, G., Martínez-Méndez, G., Stoll, H.,
595   2014. Effects of midlatitude westerlies on the paleoproductivity at the Agulhas Bank slope during the
596   penultimate glacial cycle: Evidence from coccolith Sr/Ca ratios. Paleoceanography 29.
597   https://doi.org/10.1002/2013PA002589

598 Mignot, A., Ferrari, R., Claustre, H., 2018. Floats with bio-optical sensors reveal what processes trigger the
599   North Atlantic bloom. Nat Commun 9, 1–9. https://doi.org/10.1038/s41467-017-02143-6

600 Monterey, G., Levitus, S., 1997. Seasonal Variability of Mixed Layer Depth for the World Ocean. U.S.
601   Gov. Printing Office, Wash., D.C.

602 Müller, P.J., Kirst, G., Ruhland, G., von Storch, I., Rosell-Melé, A., 1998. Calibration of the alkenone
603   paleotemperature index UK'37 based on core-tops from the eastern South Atlantic and the global
604   ocean (60°N-60°S). Geochim Cosmochim Acta 62, 1757–1772. https://doi.org/10.1016/S0016-
605   7037(98)00097-0

606 Narciso, Á., Gallo, F., Valente, A., Cachão, M., Cros, L., Azevedo, E.B., e Ramos, J.B., 2016. Seasonal
607 and interannual variations in coccolithophore abundance off Terceira Island, Azores (Central North
608 Atlantic). Cont Shelf Res 117, 43–56. https://doi.org/10.1016/J.CSR.2016.01.019

609 Newton, P.P., Lampitt, R.S., Jickells, T.D., King, P., Boutle, C., 1994. Temporal and spatial variability of
610 biogenic particles fluxes during the JGOFS northeast Atlantic process studies at 47°N, 20°W. Deep-
611 Sea Research Part I 41, 1617–1642. https://doi.org/10.1016/0967-0637(94)90065-5

612 Orsi, A.H., Whitworth, T., Nowlin, W.D., 1995. On the meridional extent and fronts of the Antarctic
613 Circumpolar Current. Deep Sea Research Part I: Oceanographic Research Papers 42, 641–673.
614 https://doi.org/10.1016/0967-0637(95)00021-W

615 Peral, M., Bassinot, F., Daëron, M., Blamart, D., Bonnin, J., Jorissen, F., Kissel, C., Michel, E., Waelbroeck,
616 C., Rebaubier, H., Gray W. R, 2022. On the combination of the planktonic foraminiferal Mg/Ca,
617 clumped ($\Delta 47$) and conventional ($\delta 18O$) stable isotope paleothermometers in palaeoceanographic
618 studies. Geochim Cosmochim Acta Preprint. https://doi.org/https://doi.org/10.31223/X5VK82

619 Poulton, A.J., Holligan, P.M., Charalampopoulou, A., Adey, T.R., 2017. Coccolithophore ecology in the
620 tropical and subtropical Atlantic Ocean: New perspectives from the Atlantic meridional transect
621 (AMT) programme. Prog Oceanogr 158, 150–170. https://doi.org/10.1016/J.POCEAN.2017.01.003

622 Prahl, F.G., Muehlhausen, L.A., Zahnle, D.L., 1988. Further evaluation of long-chain alkenones as
623 indicators of paleoceanographic conditions. Geochim Cosmochim Acta 52, 2303–2310.
624 https://doi.org/10.1016/0016-7037(88)90132-9

625 Richter, F.M., Liang, Y., 1993. The rate and consequences of Sr diagenesis in deep-sea carbonates. Earth
626 Planet Sci Lett 117, 553–565. https://doi.org/10.1016/0012-821X(93)90102-F

627 Rigual-Hernández, A.S., Trull, T.W., Nodder, S.D., Flores, J.A., Bostock, H., Abrantes, F., Eriksen, R.S.,
628 Sierro, F.J., Davies, D.M., Ballegeer, A.M., Fuertes, M.A., Northcote, L.C., 2020. Coccolithophore
629 biodiversity controls carbonate export in the Southern Ocean. Biogeosciences 17, 245–263.
630 https://doi.org/10.5194/BG-17-245-2020

631 Romero, O., Boeckel, B., Donner, B., Lavik, G., Fischer, G., Wefer, G., 2002. Seasonal productivity
632 dynamics in the pelagic central Benguela System inferred from the flux of carbonate and silicate
633 organisms. Journal of Marine Systems 37, 259–278. https://doi.org/10.1016/S0924-7963(02)00189-6

634 Shannon, L. v., Nelson, G., 1996. The Benguela: Large Scale Features and Processes and System
635 Variability, in: Wefer, G., Berger, W.H., Siedler, G., Webb, D.J. (Eds.) (Eds.), The South Atlantic:
636 Present and Past Circulation. Springer, Berlin, Heidelberg, pp. 163–210. https://doi.org/10.1007/978-
637 3-642-80353-6_9

638 Tangunan, D., Baumann, K.H., Fink, C., 2020. Variations in coccolithophore productivity off South Africa
639 over the last 500 kyr. Mar Micropaleontol 160, 101909.
640 https://doi.org/10.1016/J.MARMICRO.2020.101909

641 Tierney, J.E., Tingley, M.P., 2018. BAYSPLINE: A New Calibration for the Alkenone Paleothermometer.
642 Paleoceanogr Paleoclimatol 33, 281–301. https://doi.org/10.1002/2017PA003201

643   Tseng, C.M., Wong, G.T.F., Lin, I.I., Wu, C.R., Liu, K.K., 2005. A unique seasonal pattern in
644   phytoplankton biomass in low-latitude waters in the South China Sea. Geophys Res Lett 32, 1–4.
645   https://doi.org/10.1029/2004GL022111

646   Upadhyay, D., Lucarelli, J., Arnold, A., Flores, R., Bricker, H., Ulrich, R.N., Jesmok, G., Santi, L., Defliese,
647   W., Eagle, R.A., Carroll, H.M., Bateman, J.B., Petryshyn, V., Loyd, S.J., Tang, J., Priyadarshi, A.,
648   Elliott, B., Tripati, A., 2021. Carbonate clumped isotope analysis ($\Delta 47$) of 21 carbonate standards
649   determined via gas-source isotope-ratio mass spectrometry on four instrumental configurations using
650   carbonate-based standardization and multiyear data sets. Rapid Communications in Mass
651   Spectrometry 35, e9143. https://doi.org/10.1002/RCM.9143

652   WOA, 2018. World Ocean Atlas 2018 Data Access [WWW Document]. URL
653   https://www.ncei.noaa.gov/access/world-ocean-atlas-2018/ (accessed 4.4.22).

654

Raw coretop coccolith dataset

	Sample	Date	Mass Spec	Acid Temp	Run	d13C VPDB (Final)	d18O VPDB (Final	D47 CDES (ETF)	D47 CDES (Final)	D48 Offset	49 Param
R1	1093	2019-07-27 10:40 CEST	MAT253	70	2578	0.81	2.3	0.648	0.648	0.114	0.104
R2	1093	2019-07-27 11:29 CEST	MAT253	70	2578	0.72	2.26	0.672	0.672	-0.168	0.098
R3	1093	2019-07-29 20:13 CEST	MAT253	70	2579	0.84	2.24	0.656	0.656	-0.181	0.103
R4	1093	2019-07-29 21:01 CEST	MAT253	70	2579	0.8	2.24	0.639	0.639	-0.408	0.078
R5	1093	2019-07-29 21:48 CEST	MAT253	70	2579	0.8	2.16	0.652	0.652	-0.011	0.097
R6	1093	2019-08-01 04:53 CEST	MAT253	70	2581	0.89	2.29	0.666	0.666	-0.039	0.082
R7	1093	2019-08-01 05:41 CEST	MAT253	70	2581	0.93	2.4	0.663	0.663	-0.111	0.09
R8	1093	2019-08-01 06:29 CEST	MAT253	70	2581	0.83	2.23	0.696	0.696	-0.169	0.079
R9	1093	2020-11-03 09:49 CET	MAT253	70	2781	0.81	2.27	0.648	0.648	-0.142	0.068
R10	1093	2020-11-03 10:36 CET	MAT253	70	2781	0.9	2.32	0.688	0.688	-0.076	0.095
R11	1093	2020-11-03 11:23 CET	MAT253	70	2781	0.82	2.19	0.684	0.684	-0.009	0.093
R12	1093	2020-11-04 07:10 CET	MAT253	70	2782	0.77	2.29	0.628	0.628	-0.259	0.07
R1	1092	2019-08-13 10:30 CEST	MAT253	70	2587	3.01	3.43	0.647	0.647	0.243	0.168
R2	1092	2019-08-14 16:25 CEST	MAT253	70	2588	2.99	3.41	0.669	0.669	0.04	0.139
R3	1092	2019-08-14 17:15 CEST	MAT253	70	2588	3.01	3.47	0.623	0.623	0.095	0.188
R4	1092	2019-08-14 18:06 CEST	MAT253	70	2588	3	3.47	0.639	0.639	-0.169	0.131
R5	1092	2019-08-20 13:28 CEST	MAT253	70	2591	3.02	3.42	0.636	0.636	0.243	0.187
R6	1092	2019-08-23 20:12 CEST	MAT253	70	2595	3.01	3.54	0.696	0.696	0.241	0.112
R7	1092	2019-08-23 21:01 CEST	MAT253	70	2595	3.09	3.57	0.674	0.674	0.119	0.098
R8	1092	2019-08-23 21:48 CEST	MAT253	70	2595	3.04	3.52	0.684	0.684	0.167	0.12
R9	1092	2019-10-23 19:47 CEST	MAT253	70	2626	3.02	3.44	0.671	0.671	0.053	0.11
R10	1092	2019-10-23 20:37 CEST	MAT253	70	2626	3.02	3.55	0.656	0.656	-0.109	0.083
R11	1092	2019-10-23 21:28 CEST	MAT253	70	2626	3.04	3.42	0.649	0.649	0.127	0.115

R12	1092	2019-10-25 17:11 CEST	MAT253	70	2627	3.04	3.43	0.646	0.646	0.032	0.088
R13	1092	2019-10-25 18:00 CEST	MAT253	70	2627	3.05	3.51	0.671	0.671	-0.008	0.114
R14	1092	2019-10-25 18:47 CEST	MAT253	70	2627	3.02	3.42	0.613	0.613	-0.273	0.071
R15	1092	2019-10-27 00:58 CEST	MAT253	70	2628	3.08	3.47	0.628	0.628	-0.098	0.094
R16	1092	2019-10-27 02:40 CEST	MAT253	70	2628	3.05	3.48	0.668	0.668	-0.187	0.086
R17	1092	2019-10-29 12:22 CET	MAT253	70	2629	3.05	3.52	0.605	0.605	-0.027	0.153
R18	1092	2019-10-29 13:36 CET	MAT253	70	2629	3.01	3.55	0.707	0.707	0.069	0.149
R1	1122	2019-09-05 16:59 CEST	MAT253	70	2602	0.46	1.4	0.654	0.654	0.183	0.102
R2	1122	2019-09-05 18:40 CEST	MAT253	70	2602	0.39	1.32	0.649	0.649	-0.177	0.099
R3	1122	2019-09-07 00:21 CEST	MAT253	70	2603	0.42	1.33	0.622	0.622	0.064	0.094
R4	1122	2019-09-07 01:09 CEST	MAT253	70	2603	0.41	1.26	0.7	0.7	-0.097	0.105
R5	1122	2019-09-07 02:01 CEST	MAT253	70	2603	0.46	1.33	0.688	0.688	-0.03	0.106
R6	1122	2019-09-09 18:46 CEST	MAT253	70	2604	0.45	1.44	0.694	0.694	0.158	0.126
R7	1122	2019-09-09 20:33 CEST	MAT253	70	2604	0.45	1.41	0.619	0.619	-0.042	0.1
R8	1122	2019-09-17 15:52 CEST	MAT253	70	2606	0.52	1.46	0.642	0.642	0.144	0.129
R9	1122	2019-09-17 16:45 CEST	MAT253	70	2606	0.43	1.28	0.617	0.617	0.032	0.09
R10	1122	2020-06-25 12:28 CEST	MAT253	70	2732	0.43	1.31	0.67	0.67	-0.219	0.042
R11	1122	2020-06-25 13:15 CEST	MAT253	70	2732	0.44	1.28	0.669	0.669	-0.338	0.03
R12	1122	2020-11-04 08:59 CET	MAT253	70	2782	0.55	1.43	0.631	0.631	-0.306	0.04
R13	1122	2020-11-04 09:46 CET	MAT253	70	2782	0.46	1.32	0.655	0.655	-0.258	0.08
R1	1266	2020-01-25 04:04 CET	MAT253	70	2674	0.41	0.06	0.613	0.613	-0.197	0.034
R2	1266	2020-02-05 22:00 CET	MAT253	70	2681	0.39	0.04	0.658	0.658	-0.343	0.118
R3	1266	2020-02-05 22:53 CET	MAT253	70	2681	0.43	0.1	0.593	0.593	0.138	0.122
R4	1266	2020-02-05 23:41 CET	MAT253	70	2681	0.47	0.1	0.666	0.666	-0.271	0.121
R5	1266	2020-02-10 16:01 CET	MAT253	70	2683	0.43	0.08	0.634	0.634	-0.163	0.101
R6	1266	2020-02-10 16:48 CET	MAT253	70	2683	0.57	0.18	0.666	0.666	0.027	0.121
R7	1266	2020-02-13 05:02 CET	MAT253	70	2685	0.38	0.03	0.649	0.649	-0.073	0.067
R8	1266	2020-02-13 05:50 CET	MAT253	70	2685	0.38	0.07	0.584	0.584	0.185	0.073
R9	1266	2020-02-13 06:37 CET	MAT253	70	2685	0.46	0.1	0.662	0.662	-0.261	0.079

R10	1266	2020-02-15 21:20 CET	MAT253	70	2686	0.42	0.08	0.647	0.647	0.005	0.187
R11	1266	2020-02-15 22:08 CET	MAT253	70	2686	0.35	0.02	0.661	0.661	0.007	0.186
R12	1266	2020-02-15 22:56 CET	MAT253	70	2686	0.37	0.05	0.618	0.618	-0.004	0.185
R13	1266	2020-11-02 21:43 CET	MAT253	70	2781	0.42	0.11	0.656	0.656	-0.459	0.001
R14	1266	2020-11-02 22:30 CET	MAT253	70	2781	0.5	0.16	0.624	0.624	-0.428	0.022
R15	1266	2020-11-03 21:30 CET	MAT253	70	2782	0.54	0.18	0.668	0.668	-0.168	0.025
R16	1266	2020-11-03 22:17 CET	MAT253	70	2782	0.53	0.15	0.632	0.632	-0.326	0.009
R17	1266	2020-11-03 23:05 CET	MAT253	70	2782	0.42	0.11	0.653	0.653	-0.138	-0.003
R1	1226	2019-07-27 12:19 CEST	MAT253	70	2578	0.34	-0.59	0.61	0.61	0.414	0.117
R2	1226	2019-07-27 17:28 CEST	MAT253	70	2578	0.32	-0.63	0.624	0.624	-0.068	0.109
R3	1226	2019-07-29 22:37 CEST	MAT253	70	2579	0.35	-0.62	0.613	0.613	0.197	0.09
R4	1226	2019-07-29 23:24 CEST	MAT253	70	2579	0.31	-0.69	0.625	0.625	0.117	0.109
R5	1226	2019-07-30 00:12 CEST	MAT253	70	2579	0.3	-0.65	0.64	0.64	0.036	0.112
R6	1226	2019-08-01 07:18 CEST	MAT253	70	2581	0.36	-0.57	0.626	0.626	-0.012	0.119
R7	1226	2019-08-01 08:04 CEST	MAT253	70	2581	0.33	-0.63	0.638	0.638	0.283	0.097
R8	1226	2019-08-24 15:09 CEST	MAT253	70	2595	0.4	-0.5	0.623	0.623	0.072	0.16
R9	1226	2019-08-24 15:59 CEST	MAT253	70	2595	0.32	-0.58	0.614	0.614	0.054	0.155
R10	1226	2020-06-25 14:03 CEST	MAT253	70	2732	0.36	-0.59	0.599	0.599	-0.037	0.045
R11	1226	2020-06-25 14:53 CEST	MAT253	70	2732	0.35	-0.63	0.63	0.63	-0.2	0.032
R12	1226	2020-06-25 15:51 CEST	MAT253	70	2732	0.32	-0.63	0.613	0.613	-0.205	0.051
R1	U1338	2019-07-23 01:59 CEST	MAT253	70	2575	0.25	-1.11	0.598	0.598	0.091	0.119
R2	U1338	2019-07-23 02:49 CEST	MAT253	70	2575	0.22	-1.11	0.611	0.611	0.198	0.136
R3	U1338	2019-07-26 02:21 CEST	MAT253	70	2577	0.23	-1.14	0.612	0.612	-0.236	0.1
R4	U1338	2019-07-26 03:10 CEST	MAT253	70	2577	0.25	-1.1	0.618	0.618	-0.079	0.111
R5	U1338	2019-07-26 03:58 CEST	MAT253	70	2577	0.22	-1.17	0.596	0.596	0.119	0.107
R6	U1338	2019-07-27 05:40 CEST	MAT253	70	2578	0.25	-1.11	0.597	0.597	-0.179	0.089
R7	U1338	2019-07-27 06:30 CEST	MAT253	70	2578	0.25	-1.06	0.644	0.644	0.019	0.1
R8	U1338	2019-10-25 14:42 CEST	MAT253	70	2627	0.25	-1.11	0.596	0.596	-0.163	0.075
R9	U1338	2019-10-25 16:19 CEST	MAT253	70	2627	0.23	-1.11	0.602	0.602	0.098	0.076

R10	U1338	2019-10-26 22:35 CEST	MAT253	70	2628	0.14	-1.35	0.611	0.611	0.025	0.055
R11	U1338	2019-10-27 00:11 CEST	MAT253	70	2628	0.03	-1.54	0.591	0.591	-0.056	0.055
R1	U1337	2019-07-20 10:32 CEST	MAT253	70	2574	0.44	-0.52	0.589	0.589	0.135	0.13
R2	U1337	2019-07-20 11:22 CEST	MAT253	70	2574	0.44	-0.48	0.624	0.624	0.076	0.129
R3	U1337	2019-07-22 23:30 CEST	MAT253	70	2575	0.44	-0.49	0.607	0.607	0	0.077
R4	U1337	2019-07-23 00:17 CEST	MAT253	70	2575	0.44	-0.57	0.61	0.61	-0.073	0.09
R5	U1337	2019-07-23 01:06 CEST	MAT253	70	2575	0.45	-0.48	0.616	0.616	0.106	0.112
R6	U1337	2019-07-24 06:05 CEST	MAT253	70	2576	0.44	-0.43	0.582	0.582	0.017	0.095
R7	U1337	2019-07-24 06:52 CEST	MAT253	70	2576	0.41	-0.55	0.618	0.618	-0.209	0.1
R8	U1337	2019-07-26 00:40 CEST	MAT253	70	2577	0.44	-0.56	0.619	0.619	-0.015	0.07
R9	U1337	2019-07-26 01:28 CEST	MAT253	70	2577	0.43	-0.52	0.628	0.628	-0.01	0.101
R10	U1337	2019-10-23 11:14 CEST	MAT253	70	2626	0.42	-0.59	0.591	0.591	-0.351	0.019
R11	U1337	2019-10-23 13:00 CEST	MAT253	70	2626	0.43	-0.55	0.592	0.592	-0.162	0.052
R12	U1337	2019-10-25 12:10 CEST	MAT253	70	2627	0.43	-0.58	0.594	0.594	0.045	0.073
R13	U1337	2019-10-25 13:04 CEST	MAT253	70	2627	0.42	-0.6	0.624	0.624	-0.156	0.058
R14	U1337	2019-10-25 13:51 CEST	MAT253	70	2627	0.44	-0.57	0.596	0.596	0.003	0.082
R15	U1337	2019-10-26 20:03 CEST	MAT253	70	2628	0.44	-0.54	0.606	0.606	-0.051	0.068
R16	U1337	2019-10-26 20:54 CEST	MAT253	70	2628	0.42	-0.55	0.627	0.627	-0.195	0.061
R17	U1337	2019-10-26 21:46 CEST	MAT253	70	2628	0.44	-0.55	0.575	0.575	-0.093	0.06
R1	1143	2019-07-27 03:09 CEST	MAT253	70	2578	0.58	-1.91	0.597	0.597	0.204	0.102
R2	1143	2019-07-27 03:57 CEST	MAT253	70	2578	0.56	-2.08	0.636	0.636	0.05	0.117
R3	1143	2019-07-27 04:47 CEST	MAT253	70	2578	0.57	-1.87	0.6	0.6	0.114	0.108
R4	1143	2019-08-01 15:23 CEST	MAT253	70	2581	0.58	-1.94	0.633	0.633	0.09	0.128
R5	1143	2019-08-01 16:11 CEST	MAT253	70	2581	0.57	-2.02	0.612	0.612	-0.017	0.12
R6	1143	2019-08-01 16:59 CEST	MAT253	70	2581	0.56	-1.94	0.657	0.657	0.01	0.119
R7	1143	2019-08-09 03:19 CEST	MAT253	70	2585	0.57	-2.04	0.649	0.649	0.045	0.079
R8	1143	2019-08-09 04:11 CEST	MAT253	70	2585	0.57	-2.1	0.604	0.604	-0.119	0.127
R9	1143	2019-08-09 05:00 CEST	MAT253	70	2585	0.57	-2.09	0.658	0.658	0.168	0.132
R10	1143	2019-08-24 01:09 CEST	MAT253	70	2595	0.58	-1.97	0.597	0.597	-0.064	0.102

R11	1143	2019-08-24 01:57 CEST	MAT253	70	2595	0.59	-1.95	0.63	0.63	0.243	0.081
R12	1143	2019-08-24 02:46 CEST	MAT253	70	2595	0.59	-1.92	0.636	0.636	0.075	0.112
R13	1143	2020-11-03 02:30 CET	MAT253	70	2781	0.58	-1.9	0.643	0.643	-0.212	0.065
R14	1143	2020-11-03 03:19 CET	MAT253	70	2781	0.61	-1.97	0.636	0.636	0.139	0.048
R15	1143	2020-11-04 04:42 CET	MAT253	70	2782	0.58	-1.93	0.603	0.603	-0.1	0.066
R16	1143	2020-11-04 05:34 CET	MAT253	70	2782	0.61	-1.83	0.579	0.579	-0.082	0.033
R17	1143	2020-11-04 06:22 CET	MAT253	70	2782	0.58	-1.97	0.627	0.627	-0.239	0.049
R1	999	2019-05-23 08:17 CEST	MAT253	70	2542	0.92	-0.12	0.636	0.636	0.153	0.045
R2	999	2019-05-24 09:49 CEST	MAT253	70	2543	0.82	-0.28	0.603	0.603	-0.183	-0.032
R3	999	2019-05-24 11:24 CEST	MAT253	70	2543	0.98	-0.11	0.578	0.578	0.162	-0.021
R4	999	2019-05-27 22:17 CEST	MAT253	70	2545	0.83	-0.22	0.589	0.589	0.044	0.038
R5	999	2019-05-27 23:04 CEST	MAT253	70	2545	0.86	-0.37	0.629	0.629	0.027	0.021
R6	999	2019-05-27 23:52 CEST	MAT253	70	2545	0.84	-0.19	0.649	0.649	0.236	0.003
R7	999	2019-06-01 06:59 CEST	MAT253	70	2549	0.8	-0.29	0.588	0.588	-0.044	0.058
R8	999	2019-06-01 07:46 CEST	MAT253	70	2549	0.83	-0.41	0.612	0.612	0.11	0.026
R9	999	2019-06-01 08:34 CEST	MAT253	70	2549	0.82	-0.18	0.655	0.655	0.186	0.083
R10	999	2019-08-24 03:38 CEST	MAT253	70	2595	0.83	-0.25	0.621	0.621	0.092	0.123
R11	999	2019-08-24 04:27 CEST	MAT253	70	2595	0.87	-0.23	0.633	0.633	0.062	0.109
R12	999	2019-08-24 05:15 CEST	MAT253	70	2595	0.85	-0.31	0.618	0.618	0.143	0.118
R1	1312	2019-08-09 08:14 CEST	MAT253	70	2585	0.46	0.84	0.611	0.611	-0.173	0.093
R2	1312	2019-08-13 08:04 CEST	MAT253	70	2587	0.39	0.77	0.619	0.619	0.065	0.112
R3	1312	2019-08-13 08:51 CEST	MAT253	70	2587	0.37	0.73	0.609	0.609	0.019	0.121
R4	1312	2019-08-13 09:39 CEST	MAT253	70	2587	0.38	0.75	0.588	0.588	-0.096	0.116
R5	1312	2019-08-14 14:01 CEST	MAT253	70	2588	0.36	0.77	0.629	0.629	0.035	0.119
R6	1312	2019-08-14 14:49 CEST	MAT253	70	2588	0.34	0.72	0.599	0.599	-0.079	0.145
R7	1312	2019-08-14 15:38 CEST	MAT253	70	2588	0.31	0.74	0.666	0.666	0.12	0.198
R8	1312	2019-08-24 10:11 CEST	MAT253	70	2595	0.35	0.74	0.624	0.624	-0.165	0.135
R9	1312	2019-08-24 11:00 CEST	MAT253	70	2595	0.37	0.78	0.642	0.642	0.075	0.116
R10	1312	2019-08-24 11:48 CEST	MAT253	70	2595	0.37	0.78	0.662	0.662	0.323	0.145

R11	1312	2020-06-25 16:41 CEST	MAT253	70	2732	0.33	0.68	0.657	0.657	0.13	0.088
R12	1312	2020-06-25 17:29 CEST	MAT253	70	2732	0.45	0.86	0.66	0.66	-0.016	0.05
R13	1312	2020-06-25 18:17 CEST	MAT253	70	2732	0.37	0.74	0.625	0.625	-0.304	0.04
R14	1312	2020-11-03 04:58 CET	MAT253	70	2781	0.37	0.75	0.613	0.613	-0.355	0.03
R15	1312	2020-11-03 05:45 CET	MAT253	70	2781	0.43	0.86	0.626	0.626	0.022	0.054
R16	1312	2020-11-03 06:33 CET	MAT253	70	2781	0.36	0.76	0.629	0.629	-0.19	0.057
R17	1312	2020-11-04 02:19 CET	MAT253	70	2782	0.39	0.83	0.659	0.659	-0.161	0.048
R18	1312	2020-11-04 03:06 CET	MAT253	70	2782	0.37	0.88	0.617	0.617	-0.181	0.028
R19	1312	2020-11-04 03:54 CET	MAT253	70	2782	0.37	0.82	0.643	0.643	-0.175	0.033
R1	982	2019-07-25 21:27 CEST	MAT253	70	2577	1.35	2.15	0.625	0.625	0.053	0.126
R2	982	2019-07-27 07:18 CEST	MAT253	70	2578	1.37	2.15	0.624	0.624	0.063	0.083
R3	982	2019-07-27 08:08 CEST	MAT253	70	2578	1.34	2.15	0.645	0.645	0.07	0.11
R4	982	2019-07-27 08:56 CEST	MAT253	70	2578	1.35	2.16	0.617	0.617	-0.155	0.105
R5	982	2019-07-29 17:47 CEST	MAT253	70	2579	1.35	2.08	0.607	0.607	-0.113	0.069
R6	982	2019-07-29 18:34 CEST	MAT253	70	2579	1.41	2.13	0.681	0.681	-0.099	0.112
R7	982	2019-07-29 19:22 CEST	MAT253	70	2579	1.37	2.12	0.632	0.632	0.103	0.126
R8	982	2019-08-01 02:25 CEST	MAT253	70	2581	1.35	2.11	0.692	0.692	-0.276	0.081
R9	982	2019-08-01 03:12 CEST	MAT253	70	2581	1.35	2.14	0.698	0.698	-0.231	0.116
R10	982	2019-08-01 04:06 CEST	MAT253	70	2581	1.35	2.13	0.618	0.618	-0.031	0.085
R11	982	2019-08-09 06:35 CEST	MAT253	70	2585	1.35	2.13	0.68	0.68	-0.11	0.133
R12	982	2019-08-09 07:22 CEST	MAT253	70	2585	1.34	2.05	0.614	0.614	-0.052	0.085
R13	982	2019-08-13 02:24 CEST	MAT253	70	2587	1.36	2.11	0.641	0.641	0.065	0.139
R14	982	2019-08-24 12:37 CEST	MAT253	70	2595	1.42	2.3	0.636	0.636	0.011	0.113
R15	982	2019-08-24 14:20 CEST	MAT253	70	2595	1.35	2.2	0.654	0.654	-0.065	0.137
R16	982	2020-02-13 02:35 CET	MAT253	70	2685	1.39	2.2	0.677	0.677	-0.233	0.1
R17	982	2020-02-13 03:22 CET	MAT253	70	2685	1.4	2.26	0.663	0.663	0.038	0.12
R18	982	2020-02-13 04:10 CET	MAT253	70	2685	1.33	2.12	0.656	0.656	0.013	0.075
R19	982	2020-02-15 00:02 CET	MAT253	70	2686	1.31	2.11	0.68	0.68	0.109	0.109
R20	982	2020-02-20 23:20 CET	MAT253	70	2689	1.36	2.13	0.64	0.64	0.133	0.111
R21	982	2020-02-21 00:13 CET	MAT253	70	2689	1.43	2.22	0.659	0.659	0.121	0.152

R1	**985**	2019-08-27 15:19 CEST	MAT253	70	2596	0.05	2.01	0.654	0.654	0.257	0.182
R2	**985**	2019-08-27 17:01 CEST	MAT253	70	2596	-0.03	1.95	0.688	0.688	0.19	0.183
R3	**985**	2019-08-28 16:18 CEST	MAT253	70	2597	-0.02	1.99	0.614	0.614	0.129	0.153
R4	**985**	2019-08-28 17:06 CEST	MAT253	70	2597	-0.01	1.94	0.609	0.609	-0.114	0.132
R5	**985**	2019-08-28 17:55 CEST	MAT253	70	2597	0.02	2	0.608	0.608	0.115	0.142
R6	**985**	2019-08-30 10:15 CEST	MAT253	70	2598	0.03	2.05	0.613	0.613	0.123	0.122
R7	**985**	2019-09-07 02:48 CEST	MAT253	70	2603	0.02	1.96	0.645	0.645	0.166	0.104
R8	**985**	2019-09-07 03:42 CEST	MAT253	70	2603	-0.04	1.94	0.649	0.649	0.095	0.081
R9	**985**	2019-09-07 04:29 CEST	MAT253	70	2603	0.01	1.98	0.663	0.663	0.24	0.104
R10	**985**	2020-06-25 19:08 CEST	MAT253	70	2732	-0.05	1.93	0.674	0.674	-0.139	0.087
R11	**985**	2020-06-25 20:05 CEST	MAT253	70	2732	-0.08	1.85	0.634	0.634	-0.431	0.085
R12	**985**	2020-06-25 20:53 CEST	MAT253	70	2732	-0.06	1.84	0.62	0.62	-0.075	0.076